

# Nitric oxide coordinates growth, development, and stress response via histone modification and gene expression

Alexandra Ageeva-Kieferle,<sup>1</sup> Elisabeth Georgii ,<sup>1</sup> Barbro Winkler ,<sup>2</sup> Andrea Ghirardo ,<sup>2</sup> Andreas Albert ,<sup>2</sup> Patrick Hüther,<sup>3</sup> Alexander Mengel,<sup>1</sup> Claude Becker ,<sup>3,4</sup> Jörg-Peter Schnitzler ,<sup>2</sup> Jörg Durner<sup>1,5</sup> and Christian Lindermayr ,<sup>1,\*†</sup>

<sup>1</sup> Institute of Biochemical Plant Pathology, Helmholtz Zentrum München, Neuherberg 85764, Germany

<sup>2</sup> Research Unit Environmental Simulation, Helmholtz Zentrum München, Neuherberg 85764, Germany

<sup>3</sup> Gregor Mendel Institute of Molecular Plant Biology, Austrian Academy of Sciences, Vienna BioCenter (VBC), Vienna 1030, Austria

<sup>4</sup> Faculty of Biology, Ludwig-Maximilians-University Munich, LMU Biocenter, Martinsried 82152, Germany

<sup>5</sup> Chair of Biochemical Plant Pathology, Technische Universität München, Freising 85354, Germany

\*Author for communication: lindermayr@helmholtz-muenchen.de

†Senior author.

A.A. and C.L. conceived research plans; C.L., B.W., A.G., A.Al., and C.B. supervised the experiments; A.A., P.H., and A.M. performed the experiments; A.A., C.L., E.G., B.W., A.G., and A.Al. designed the experiments and analyzed the data; A.A. and C.L. wrote the article with contributions of all the authors; E.G., A.G., C.B., J.-P.S., and J.D. reviewed and edited the text. C.L. agrees to serve as the author responsible for contact and ensures communication.

The author responsible for distribution of materials integral to the findings presented in this article in accordance with the policy described in the Instructions for Authors (<https://academic.oup.com/plphys/pages/general-instructions>) is: Christian Lindermayr (lindermayr@helmholtz-muenchen.de).

## Abstract

Nitric oxide (NO) is a signaling molecule with multiple regulatory functions in plant physiology and stress response. In addition to direct effects on transcriptional machinery, NO executes its signaling function via epigenetic mechanisms. We report that light intensity-dependent changes in NO correspond to changes in global histone acetylation (H3, H3K9, and H3K9/K14) in *Arabidopsis* (*Arabidopsis thaliana*) wild-type leaves, and that this relationship depends on S-nitrosoglutathione reductase and histone deacetylase 6 (HDA6). The activity of HDA6 was sensitive to NO, demonstrating that NO participates in regulation of histone acetylation. Chromatin immunoprecipitation sequencing and RNA-seq analyses revealed that NO participates in the metabolic switch from growth and development to stress response. This coordinating function of NO might be particularly important in plant ability to adapt to a changing environment, and is therefore a promising foundation for mitigating the negative effects of climate change on plant productivity.

## Introduction

Nitric oxide (NO) is a ubiquitous signaling molecule with pleiotropic functions that operates throughout the lifespan of plants. Indeed, NO is involved in several physiological processes, including growth and development, but also in iron

homeostasis, as well as biotic and abiotic stress responses, such as to high salinity, drought, ultraviolet-B radiation, high temperature, and heavy metal toxicity (Delledonne et al., 1998; Durner et al., 1998; Mata and Lamattina, 2001; Zhao et al., 2004, 2007; An et al., 2005; Tian et al., 2007; Besson-

Bard et al., 2009; Puyaubert and Baudouin, 2014). NO is a heteronuclear diatomic radical with a half-life of 3–5 s in biological systems, and the multifunctional role of NO is based on its chemical properties, cellular environment, and compartmentalization. Depending to a large extent on its local concentration, which is affected by its rate of synthesis, displacement, and removal, NO has been described as a cytoprotective, signaling, or cytotoxic molecule (Floryszak-Wieczorek et al., 2006; Mur et al., 2013; Yu et al., 2014; Buet and Simontacchi, 2015; Trapet et al., 2015; Fancy et al., 2017; Ageeva-Kieferle et al., 2019).

NO fulfills its biological functions by modulating protein function/activity through different types of posttranslational modifications (PTMs): protein S-nitrosation, tyrosine nitration, or metal nitrosylation. Protein S-nitrosation—the covalent attachment of NO to the sulfur group of cysteine residues—is one of the most important NO-dependent protein modifications, and plants respond to many different environmental changes by S-nitrosating a specific set of proteins (Romero-Puertas et al., 2008; Puyaubert et al., 2014; Vanzo et al., 2016; Jain et al., 2018). S-Nitrosated glutathione (S-nitrosoglutathione, GSNO) has important functions as an NO reservoir, NO transporter, and physiological NO donor that can transfer its NO moiety to protein cysteine residues (Hess et al., 2005; Kovacs and Lindermayr, 2013). Therefore, the level of S-nitrosated proteins corresponds to GSNO levels. The level of GSNO is controlled by the catalytic activity of GSNO reductase (GSNOR; EC: 1.1.1.284). This enzyme catalyzes the degradation of GSNO to oxidized glutathione and ammonium, and in this way, directly regulates the level of GSNO, and indirectly regulates the level of S-nitrosated proteins (Liu et al., 2001; Sakamoto et al., 2002). Loss of GSNOR function results in enhanced levels of low and high molecular S-nitrosothiols (SNOs; FeechAn et al., 2005; Lee et al., 2008; Kovacs et al., 2016). The pleiotropic phenotype of GSNOR-knock-out mutants (backgrounds Columbia and Wassilewskija) and their sensitivity to biotic and abiotic stress clearly demonstrate the importance of this enzyme for plant growth, development, and stress response (FechAn et al., 2005; Lee et al., 2008; Holzmeister et al., 2011; Wünsche et al., 2011; Kwon et al., 2012; Xu et al., 2013).

Using a site-specific nitrosoproteomic approach, several hundred target proteins for S-nitrosation were identified in *Arabidopsis gsnor* plants (Hu et al., 2015). These proteins are involved in a wide range of biological processes including chlorophyll metabolism and photosynthesis. Consistently, *gsnor* mutants exhibited altered photosynthetic properties, such as increased quantum efficiency of photosystem II (PSII) photochemistry and photochemical quenching, and decreased nonphotochemical quenching (Hu et al., 2015), suggesting that S-nitrosation is an important regulatory mechanism for light-dependent processes. In several studies, *gsnor* plants were analyzed on proteome and transcriptome levels to gain insights into the physiological functions of this enzyme (Fares et al., 2011; Holzmeister et al., 2011; Kovacs et al., 2016; Kuruthukulangarakoola et al., 2017).

Gene transcription can be regulated via modification of transcription factors or via chromatin modifications. The chromatin structure in eukaryotic organisms is very dynamic and changes in response to environmental stimuli. Chromatin marks are defined modifications on histone tails or DNA, playing key roles in processes such as gene transcription, replication, repair, and recombination (Bannister and Kouzarides, 2011). DNA methylation is usually associated with long-term silencing of genes, whereas histone modifications contribute to both activation and repression of gene transcription, and are mostly removed after several cell cycles (Jaenisch and Bird, 2003; Minard et al., 2009). Several lines of evidence demonstrate that NO regulates gene expression via modification of the chromatin structure and/or DNA accessibility. In general, the distinct chromatin states that modulate access to DNA for transcription are regulated by multiple epigenetic mechanisms, including DNA methylation, covalent modifications (such as methylation and acetylation) of core histones, ATP-dependent chromatin remodeling, placement of histone variants, noncoding RNAs, and metabolo-epigenetic effects (Schvartzman et al., 2018; Zhang et al., 2018; Lindermayr et al., 2020). Recently, we demonstrated that NO affects histone acetylation by targeting and inhibiting histone deacetylase (HDA, EC: 3.5.1.98) complexes, resulting in the hyperacetylation of specific genes (Mengel et al., 2017). Treatment with the physiological NO donor GSNO increased global histone H3 (H3) and H4 acetylation. Chromatin immunoprecipitation sequencing (ChIP-seq) revealed that several hundred genes displayed NO-regulated histone acetylation. Many of these genes were involved in plant defense response and abiotic stress response, but also in chloroplast function, suggesting that NO might regulate expression of specific genes by modulating chromatin structure (Mengel et al., 2017).

*Arabidopsis* contains 18 isoforms of HDAs, divided into three subfamilies: Reduced Potassium Deficiency 3 (RPD3)-like, HD-tuins and sirtuins (Hollender and Liu, 2008). The first subfamily is the largest, and is composed of 12 putative members (HDA2, HDA5–10, HDA14–15, HDA17–19), which, based on structural similarity, can be further divided into three classes. HDAs of this type are homologous to yeast RPD3 proteins that are ubiquitous in all eukaryotes. All members of this subfamily contain a specific deacetylase domain that is required for their catalytic activity. The second subfamily contains the HD-tuins (HD2), and was originally found in maize. This type of proteins is plant-specific, although homologous cis-trans prolyl isomerases are also present in other eukaryotes (Dangl et al., 2001). The third subfamily of plant HDAs is represented by sirtuins (SIR2-like proteins), which are homologous to yeast silent information regulator 2 (SIR2; Pandey et al., 2002). These HDAs are unique because they require a NAD cofactor for functionality, and unlike RPD3 proteins, they are not inhibited by trichostatin A (TSA) or sodium butyrate. Moreover, sirtuins use a wide variety of substrates beyond histones.

Here, we report that increased light intensity (dark conditions, 200  $\mu\text{mol}$  photons  $\text{m}^{-2} \text{s}^{-1}$ , or 1,000  $\mu\text{mol}$  photons  $\text{m}^{-2} \text{s}^{-1}$ ) enhances NO/SNO levels in *Arabidopsis* leaves.

These light intensity-dependent changes in SNO/NO levels correspond to changes in global H3 acetylation and acetylation of H3K9 and H3K9/K14 in *Arabidopsis* wild-type (wt) plants. Interestingly, there were no light intensity-dependent changes in histone acetylation observed in plants with loss of GSNOR (*gsnor1-3*; [FeechAn et al., 2005](#); [Lee et al., 2008](#)) or HDA6 (called *hda6* or *axe1-5*; [Murfett et al., 2001](#); [Wu et al., 2008](#)), a member of the RPD3-like subfamily, suggesting a light intensity-dependent regulatory function of GSNOR and HDA6 on histone acetylation. In vitro measurement of enzyme activities provided evidence that *Arabidopsis* HDA6 is sensitive to NO. A ChIP-seq analysis of the H3K9ac mark in wt and mutants *gsnor* and *hda6* under dark and low light (LL) conditions identified 16,276 acetylated loci. Interestingly, under LL, GSNOR, and HDA6 share a substantial function in deacetylation of genes involved in growth/development, and acetylation of stress-responsive genes, suggesting a link between GSNOR (level of SNO) and HDA6 in these functions. Furthermore, RNA-seq analysis of wt, *gsnor*, and *hda6* mutants under dark and low-light conditions revealed a common function of GSNOR and HDA6 in downregulation of genes involved in growth/development and at the same time, upregulation of stress-related genes. In summary, our data suggest a function for NO as molecular switch between growth/development on one side and stress responses on the other side.

## Results

### Enhanced light-dependent production of NO/SNO in *Arabidopsis* plants with loss of GSNOR function

In plants, both NO and radiation are important regulators of growth, development and stress response. To further demonstrate a link between light and NO/SNOs, we analyzed NO emission of single *Arabidopsis* plants under different light intensities in a closed cuvette using a CLD Supreme NO analyzer. Only very small differences in NO emission between LL (photosynthetic photon flux density (PPFD) of 200- $\mu\text{mol}$  photons  $\text{m}^{-2} \text{s}^{-1}$ , T 22°C) and dark (D, PPFD of 0  $\mu\text{mol}$  photons  $\text{m}^{-2} \text{s}^{-1}$ , T 22°C) conditions were observed in *Arabidopsis* wt plants ([Figure 1A](#)). Probably, the changes in NO emission under these conditions were below the detection limit of the NO analyzer.

In contrast, simulation of sunflecks, that is, transient exposure to high light (HL, PPFD of 1,000  $\mu\text{mol}$  photons  $\text{m}^{-2} \text{s}^{-1}$ ) in combination with increased temperature (T 30°C) led to a substantial increase in emission of NO in wt plants (approximately five-fold) in comparison to LL/low temperature conditions (LL, 200  $\mu\text{mol}$  photons  $\text{m}^{-2} \text{s}^{-1}$ , T 22°C; [Figure 1B](#)). The increase in NO emission was higher in plants with loss of GSNOR activity (*gsnor*; approximately two-fold) in comparison to wt plants ([Figure 1B](#)). Increase of temperature alone did not enhance NO emission ([Figure 1B](#)), while HL intensity in a constant temperature substantially increased NO emission ([Figure 1C](#)), demonstrating a link between light intensity and NO emission independent of temperature.

As differences in NO emission could result from differences in stomata opening, endogenous SNO and nitrite contents were determined in *Arabidopsis* leaves. Plants were grown for 4 weeks under short day, low temperature (22°C), and LL conditions. After exposure for 4 h to LL, plants were transferred for 4 h to darkness (D, T 22°C) or high PPFD (HL, 1,000  $\mu\text{mol}$  photons  $\text{m}^{-2} \text{s}^{-1}$ , T 30°C), or kept under low PPFD (LL, 200  $\mu\text{mol}$  photons  $\text{m}^{-2} \text{s}^{-1}$ , T 22°C) conditions ([Figure 1D](#)). Afterwards, SNO and nitrite contents were determined. In general, SNO content was higher in *gsnor* than in wt plants ([Figure 1E](#)). When kept under LL intensity, the SNO content in wt and *gsnor* plants was 45 and 88 fmol  $\mu\text{g}^{-1}$  protein, respectively. In both lines, the SNO level did not significantly increase when plants were transferred to HL intensity. However, plants transferred to darkness exhibited significantly lower SNO levels than plants kept under low or high PPFD intensities (wt: 45–19 fmol  $\mu\text{g}^{-1}$  protein, *gsnor*: 88–44 fmol  $\mu\text{g}^{-1}$  protein), further demonstrating a link between SNO formation and light intensity. Nitrite content is a frequently used option to infer NO accumulation ([He et al., 2004](#); [Holzmeister et al., 2011](#)). The nitrite levels under the different irradiation conditions corresponded to the SNO contents for *gsnor* and wt plants ([Figure 1F](#)). Within the different PPFD levels, wt and *gsnor* plants did not significantly differ in their nitrite contents, but significantly lower nitrite levels were detected in both wt and *gsnor* plants when transferred to the dark. In addition, endogenous SNO levels of 4-week-old plants grown under short-day conditions (10/14-h light/dark, 20°C/17°C) were determined at different time points during the light and dark period ([Figure 1G](#)). A tendency toward enhanced SNO concentration was observed under light, whereas lower SNO amounts were measured in the dark-treated plants, further confirming a light-dependent accumulation of SNOs. Loss of GSNOR function resulted in slightly higher SNO levels in comparison to wt ([Figure 1G](#)).

### GSNOR regulates histone acetylation in plants transferred to dark and two different light conditions

Previously, we demonstrated that exogenously applied NO donors and endogenously induced NO production results in enhanced histone acetylation ([Mengel et al., 2017](#)). Therefore, we analyzed whether light-dependent accumulation of NO/SNO also leads to chromatin remodeling in wt and *gsnor* plants. Four-week-old plants of both lines were exposed to different light conditions as mentioned above (section “Enhanced light-dependent production of NO/SNO in *Arabidopsis* plants with loss of GSNOR function”), and global leaf levels of H3ac, H3K9ac, and H3K9/14ac histone marks were quantified by immunoblotting using histone mark-specific antibodies ([Figure 2, A–D](#)). Here, wt plants showed a tendency towards a continuous increase in H3ac and H3K9/14ac levels from D to LL to HL conditions ([Figure 2, B and D](#)). We observed significant increases of ~2.5-fold and 2-fold under HL conditions compared to D conditions for H3ac and H3K9/14ac, respectively ([Figure 2, B and D](#)).

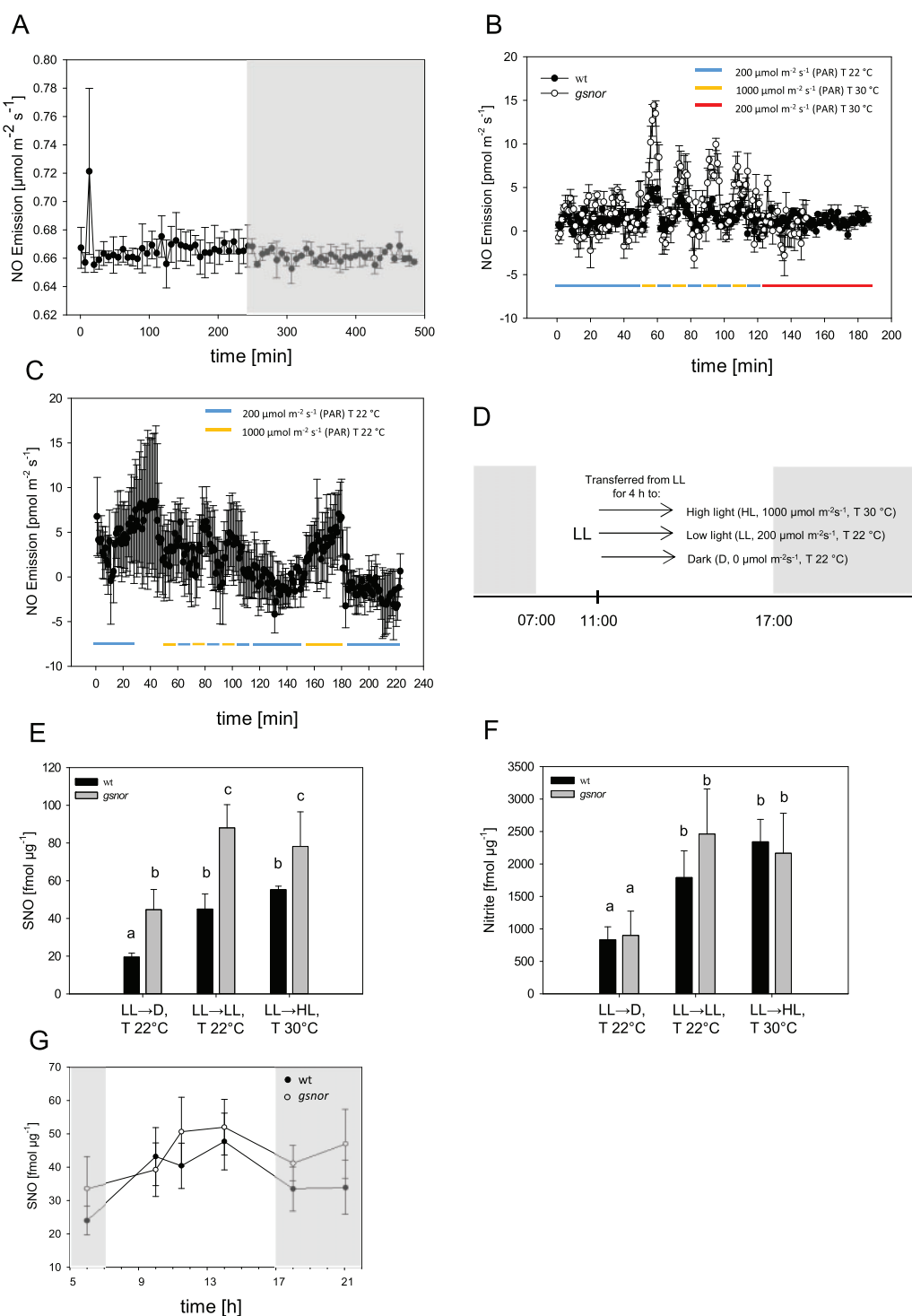


**Figure 1** Light-dependent NO emissions and nitrite and S-nitrosothiol accumulation in Arabidopsis plants. A–C, NO emission of single Arabidopsis plants. Plants were placed in an Arabidopsis cuvette and NO emission was measured by chemiluminescence using an ultra-high sensitive NO analyzer. Temperature and dark and light conditions were applied as indicated. Light intensity is given as PPFD ( $\mu\text{mol photons m}^{-2} \text{s}^{-1}$ ). Means  $\pm$  SE of at least three independent experiments ( $N \geq 3$ ) are shown. D, Experimental setup for treatments with different light conditions. Four-week-old plants grown on soil under short day cycles (10/14 h light/dark, 20/17 °C) were transferred at noon (11:00) for 4 h to dark (D, T 22 °C), LL (T 22 °C), or HL (T 30 °C). E–G, Determination of S-nitrosothiol and nitrite content after exposure to different light conditions. Total S-nitrosothiol (E) and nitrite (F) levels were determined after 4 h. Means  $\pm$  SE of three independent experiments ( $N = 3$ ) are shown. Letters are assigned to bars based on one-way analysis of variance (ANOVA) with Tukey's post hoc test. Two-way ANOVA results: in (E) difference among light and temperature conditions –  $P = 0.009$ , difference between wt and gsnor mutant –  $P = 0.004$ . Pairwise comparisons were performed using the Holm-Sidak test: D versus HL –  $P = 0.020$ , D versus LL –  $P = 0.014$ . In (F) difference among light and temperature conditions –  $P = 0.011$ . Pairwise comparisons: D versus HL –  $P = 0.017$ , D versus LL –  $P = 0.029$ . G, Total S-nitrosothiol levels of wt and gsnor plants were determined at 06:00, 10:00, 11:30, 14:00, 18:00, and 21:00. The light period was from 07:00 to 17:00. Means  $\pm$  SE of at least three independent experiments ( $N \geq 3$ ) are shown. Shaded portions in the graph represent dark conditions.

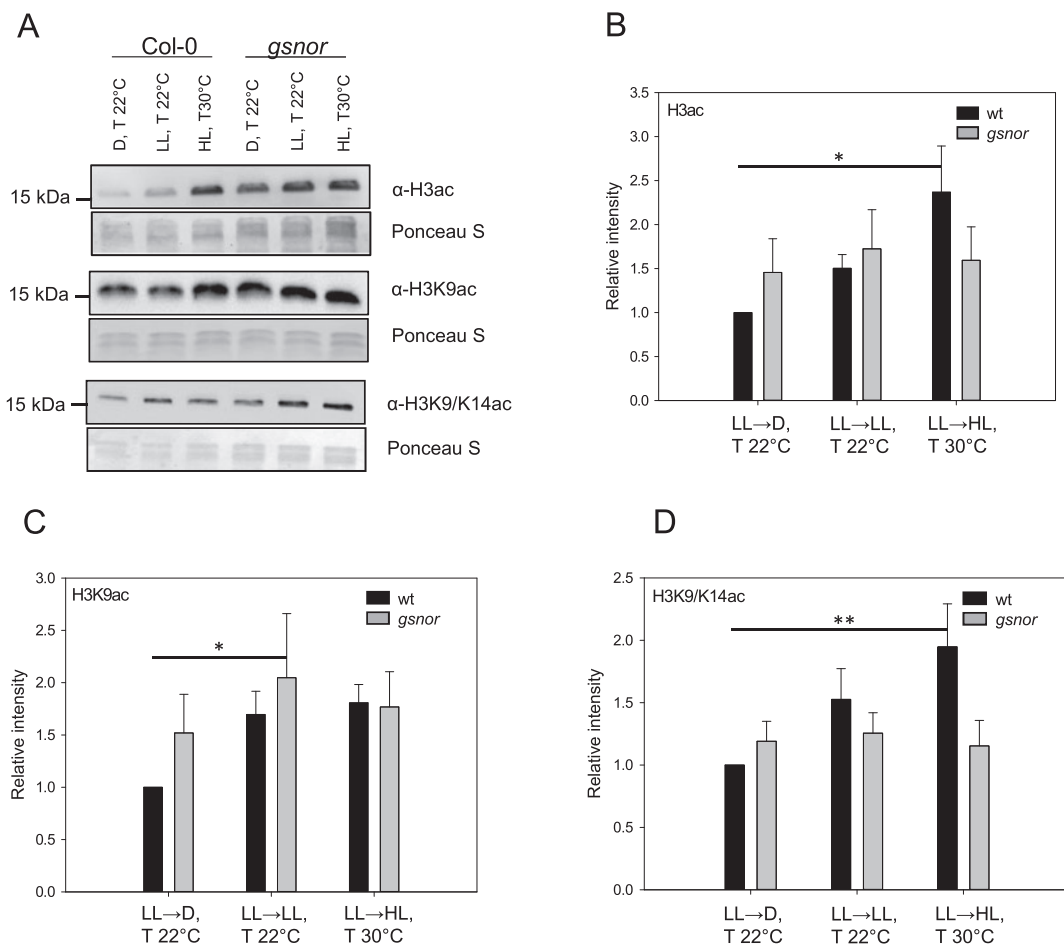


**Figure 2** Different light conditions lead to altered H3 acetylation in wt and *gsnor* plants. **A**, Immunoblot detection of histone modifications. Four-week-old plants were exposed for 4 h to the indicated light conditions. Histones were extracted and analyzed for the indicated histone marks. **B–D**, Quantitative analyses of the immunodetected bands of the different histone marks. Signal intensity was determined with Image J software. The mean  $\pm$  se of at least five independent experiments ( $N \geq 5$ ) is shown. Intensities are given relative to the histone acetylation level in wt under D conditions, which was set to 1. Significant deviations from this constant were determined by Holm adjustment after one-way ANOVA (\*\* $P \leq 0.01$ , \* $P \leq 0.05$ ).

Moreover, the H3K9ac level tended to be higher in HL conditions in comparison to D, being close to significance (Figure 2C, adjusted  $P$ -value 0.053). Scavenging of HL-induced NO with 2-4-carboxyphenyl-4,4,5,5-tetramethylimidazoline-1-oxyl-3-oxide (cPTIO) confirmed the relationship between NO and histone acetylation (Supplemental Figure S1). In *gsnor* plants, total H3ac, H3K9ac, and H3K9/14ac levels were similar across the different light conditions, and in most cases, not significantly higher than the wt D level (Figure 2, B–D). Thus, the correspondence of histone acetylation to light intensity observed in wt was not present in *gsnor* plants. These data demonstrate that disturbed SNO homeostasis affects dark/light-dependent histone acetylation, suggesting a regulatory function of GSNOR (SNOs) in histone acetylation under these conditions.

#### Identification of putative NO-sensitive HDAs

In Mengel et al. (2017), we demonstrated that total HDA activity is reversibly inhibited in vitro by different NO donors (GSNO and SNAP), and in vivo by SA and INA, which both

stimulate endogenous NO accumulation. However, it is still unclear which of the 18 different Arabidopsis HDAs are sensitive to NO. Members of the RPD3-like subfamily are the most promising candidates since this subfamily includes HDA homologues to human HDA2. Mammalian HDA2 is S-nitrosated at Cys262 and Cys274 in response to NO, resulting in chromatin remodeling in neurons and in dystrophic muscles (Colussi et al., 2008; Nott et al., 2008).

Comparison of the amino acid sequences of human HDA2 and Arabidopsis RPD3-like enzymes revealed that HDA6 is the closest homolog to human HDA2, with a sequence identity of 61%. Both proteins contain seven conserved Cys, which are located within the HDA domain, including two Cys residues (Cys273 and Cys285 of AtHDA6) that correspond to the S-nitrosated Cys residues in mammalian HDA2 (Figure 3A). Interestingly, the bioinformatic prediction tool GPS-SNO found that Cys273 of Arabidopsis HDA6 is a predicted target for S-nitrosation (Xue et al., 2010). Structural modeling of Arabidopsis HDA6 using the crystal structure of human HDA2 as template revealed

A	Hs HDA2	-----MAYSQGGGKKKVCYYYYDGDIGNYYYGQGHPMKPHRIRMTHNLLNYGLYRK	51
	Ath HDA6	MEADESGISLPSGPDRKRRLRSVSYFYEPTIGDYYYGQGHPMKPHRIRMAHSLIHYHLRR	60
	Hs HDA2	MEIYRPHKATAEEMTKYHSDEYIKFLRSIRPDNMSEYS--KQMQRFNVGEDCPVFDGLFE	109
	Ath HDA6	LEISRSPSLADASDIGHRFHSPEYVDFLASVSPESMGPSAARNLRRFNVGEDCPVFDGLFD	120
	Hs HDA2	FCQLSTGGSVAGAVKLNRQQTDMAVNWAGGLHHAKKSEASGF	169
	Ath HDA6	FCRASAGGSIGAAVKLNLRQDADIAINWGGGLHHAKKSEASGF	180
	Hs HDA2	RVLYIDIDIHGDGVEEAFYTTDRVMTVSFSHKYGEYFPGTGDLRDIGAGKGKYYAVNFPM	229
	Ath HDA6	RDGIDDESQYQGQIFKPIISKVMEEMYQPSAVVLQCGADSLSGDRLGC	289
		CFNLTVKGHAKCVEVV	
	Hs HDA2	NDGMDDESFRSLFRPLIQKVMEVYQPEAVVLQCGADSLSGDRLGC	300
	Ath HDA6	CFNLSVKGHADCLRFL	
	Hs HDA2	KTFNLPPLMLGGGGYTIRNVAR	349
	Ath HDA6	CWTYETAVALDCEIPNELYNDYFEYFGPDFKLHISPS	360
	Hs HDA2	RSYNVPMLVGGGYTIRNVAR	
	Ath HDA6	WCYETAVAVGVEPDNKLPNEYFEYFGPDYTLHVDPS	
	Hs HDA2	NMTNQNTPEYMEKIKQQLRFENLRLMPHAPGVQMIAIPEDAHDGDEDGEDPDKRISIR	409
	Ath HDA6	PMENLNTPKDMERIRNTLLEQLSGLIAPSQFOHTPPVRNRVLDPEDDMETRPK----	415
	Hs HDA2	ASDKRIACDEEFSDEDEGEGGRRNVADHKKGAKKARIEEDKKTEDKKTDVKEEDKSKD	469
	Ath HDA6	---PRIWSGTATYESSDDDDKPLHGYSRCRGATTDRDSTGEDEMDD---DNPEPDVNPP	469
	Hs HDA2	NSGEKTDTKGKSEQLSNP	488
	Ath HDA6	SS-----	471

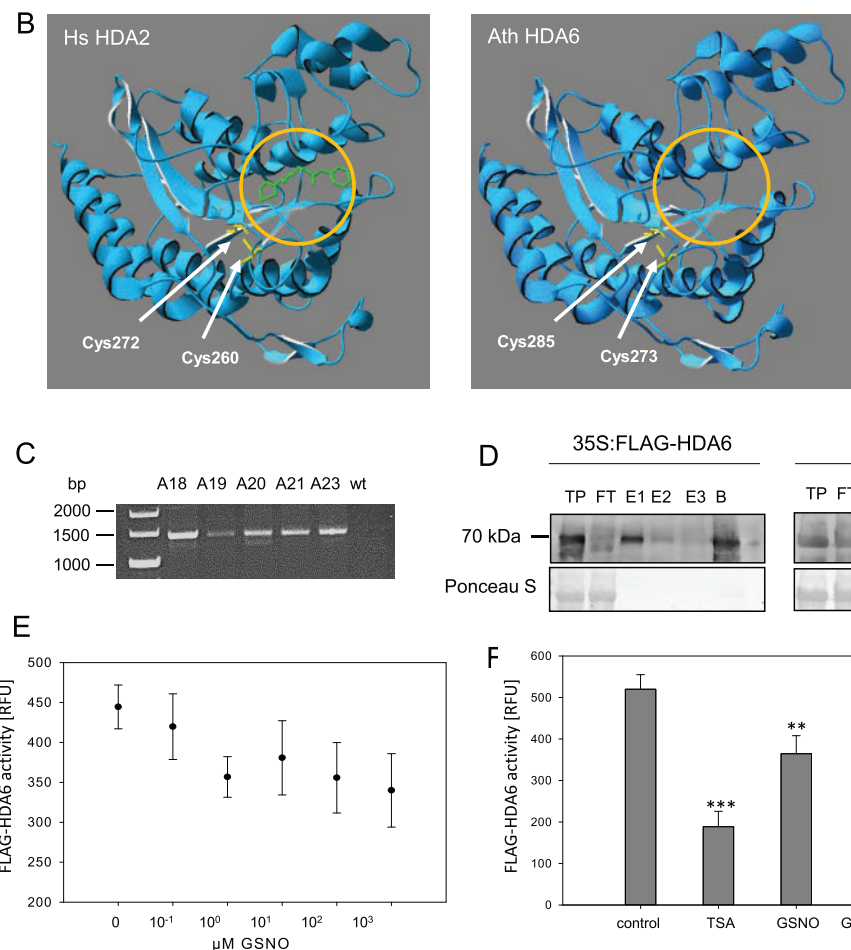


**Figure 3** S-Nitrosation of *Arabidopsis* HDA6. **A**, Amino acid sequence alignment of human HDA2 and *Arabidopsis* HDA6. The alignment was performed using Clustal Omega. Cysteine residues that are S-nitrosated in human HDA2 are marked in red, other conserved cysteines are indicated in yellow. HDA region is highlighted in gray. **B**, Structural modeling of *Arabidopsis* HDA6. The HDA domain of *Arabidopsis* HDA6 (amino acids 18–386, Uniprot entry Q9FML2) was modeled using the SwissProt Modeling server with human HDA2 as a template (PDB code: 4LXZ). The 3D models were visualized with Swiss-PdbViewer. Cysteine residues that are S-nitrosylated in human HDA2, as well as the corresponding putative redox-sensitive cysteines of HDA6, are indicated in yellow. The bound HDAC inhibitor suberanilohydroxamic acid (green) in human HDA2 indicates its active center, which is highlighted in each enzyme with an orange circle. Recombinant FLAG-HDA6 was produced in *Arabidopsis*. **C**, RT-PCR of transgenic 35S:FLAG-HDA6 *Arabidopsis* lines. Five 35S:FLAG-HDA6-containing lines, A18–A21, and A23, were identified. cDNA of wt was used as a negative control. Predicted size of FLAG-HDA6 is around 1,470 bp. **D**, Immunoblot of plant-produced FLAG-HDA6. Total protein (TP) of the transgenic line A18 and wt was subjected to FLAG resin and recombinant protein was eluted three times (E1–E3). TP, flow-through (FT), E1–E3, and boiled beads (B) were analyzed by immunoblotting. Anti-FLAG-tag antibody (1:1,000) was used for immunodetection. Predicted size of FLAG-HDA6 is 57 kDa. One representative experiment of at least three replicates is shown. **E**, Inhibition of FLAG-HDA6 activity by GSNO. The

strikingly similar 3D folds of both proteins (Figure 3B). In the structural model of *Arabidopsis* HDA6, Cys273, and Cys285 are located at the same positions as the S-nitrosated Cys262 and Cys274 in the 3D structure of human HDA2 (Figure 3B), indicating that both proteins exhibit a very similar microenvironment around the substrate binding site.

An *hda6* cell suspension line was generated to determine whether NO-dependent inhibition of total HDA activity is altered upon the knockout of HDA6. The *hda6* allele (also called *axe1-5*) used to generate the cell culture contained an insertion resulting in a premature stop codon and the expression of a nonfunctional, C-terminally truncated version of the HDA6 protein (Murfett et al., 2001). Cell cultures exhibited similar growth kinetics and morphology to wt cells. Consistent with previous results (Mengel et al., 2017), wt cells showed a slight but significant increase in total H3ac level after GSNO treatment (500 μM), and a more pronounced, ~2.5-fold increase after TSA application (Supplemental Figure S2; Mengel et al., 2017). In contrast, GSNO treatment of *hda6* cells did not result in an accumulation of acetylated H3 (Supplemental Figure S2). TSA treatment did not increase the rate of H3 acetylation either, indicating that HDA6 was the predominant TSA-sensitive HDA isoform in this cell culture system. Moreover, HDAC activity in wt nuclear extracts was sensitive to NO, but TSA treatment could not completely abrogate HDAC activity (residual activity of 65%; Supplemental Figure S3), indicating the presence of TSA insensitive HDACs (i.e. sirtuins). HDAC activity in *hda6* nuclear extracts was around 50% lower than in wt nuclear extracts (Supplemental Figure S3) and—consistent with the western blot results (Supplemental Figure S2)—was insensitive to N-ethylmaleimide, a cysteine blocking compound (Supplemental Figure S4). These data imply that HDA6 is a promising candidate for a NO-sensitive HDA isoform.

To analyze if HDA6 can be S-nitrosated in vitro and if S-nitrosation indeed affects its activity, HDA6 protein was recombinantly produced in *Escherichia coli* BL21(DE3) cc4—a strain which contains additional chaperones that help to produce proteins with low solubility—as His<sub>6</sub>-HDA6 and GST-HDA6. However, no deacetylase activity could be measured for His<sub>6</sub>-HDA6 and GST-HDA6. We thus speculate that HDA6 might need certain PTMs or interaction partner(s) to function as an active HDA. We therefore produced recombinant FLAG-HDA6 in *Arabidopsis*. The presence of FLAG-HDA6 transcripts in transgenic lines were demonstrated by reverse transcription polymerase chain reaction (RT-PCR) (Figure 3C). We purified recombinant FLAG-HDA6 protein and confirmed via immunoblot the presence of

recombinant FLAG-HDA6, with a predicted size around 55 kDa, in transgenic lines (Figure 3D).

Activity measurements demonstrated that recombinant FLAG-HDA6 was produced in a catalytically active form (Figure 3E). Treatment with increasing concentration of GSNO (up to 1,000 μM) resulted in ~30% inhibition of FLAG-HDA6 activity (Figure 3E), whereas 1-μM TSA reduced the activity by 65% (Figure 3F). Surprisingly, the activity of GSNO-treated FLAG-HDA6 could not be restored by subsequent treatment with 5-mM DTT; in contrast, addition of DTT further inhibited HDA6 activity by 30% (Figure 3F). Taken together, these data imply that HDA6 a promising candidate for a NO-affected HDA isoform.

### HDA6 regulates histone acetylation in plants transferred to dark and two different light conditions

As demonstrated above, exposure to increasing light intensities enhanced NO emissions and SNO accumulation (Figure 1). As HDA6 is inhibited by NO/SNO, we investigated whether biochemical function of HDA6 is required for regulating histone acetylation under dark and light conditions. Total H3ac, H3K9ac, and H3K9/14ac levels in *hda6* knockout plants (also named *axe1-5*) were analyzed under the different light conditions described above for *gsnor* (Figure 1D).

H3K9ac and H3K9/14ac are known substrates for HDA6 (Luo et al., 2015). As shown in Figure 4, total H3ac, H3K9ac, and H3K9/14ac levels significantly increased from D to HL conditions in wt plants (Figure 4, A–D). Interestingly, the acetylation levels in *hda6* (H3ac, H3K9ac, and H3K9/14ac)—similarly to the acetylation levels in *gsnor*—did not follow this trend. Under HL conditions, the acetylation levels of the analyzed histone marks are very similar between wt and *hda6*, while under LL and dark conditions, the acetylation levels tended to be higher in *hda6* plants. Actually, in the dark, H3K9/14ac levels showed a significant 3.5-fold increase in *hda6* in comparison to wt. These data indicate that like GSNOR activity, HDA6 activity is involved in modulating the chromatin structure, especially in the dark and under LL intensities.

### Profiling of H3K9ac marks in light and dark conditions reveals differences between *gsnor* and *hda6* relative to wt

Under LL intensities, and especially when plants were transferred to the dark, histone deacetylation of H3, H3K9, and H3K9/14 depended on both GSNOR and HDA6 activities (Figures 2, 4). To identify chromatin regions regulated by

recombinant plant FLAG-HDA6 was incubated with 0.1–1,000 μM GSNO for 20 min and its activity was determined. Mean ± se of three independent experiments ( $N = 3$ ) is shown (F) Activity of FLAG-HDA6 after treatment with 1 μM TSA, 1 mM GSNO and 1 mM GSNO/5 mM DTT. HDA activity was measured using Fluorogenic HDA Activity Assay. Mean ± se of at least three independent experiments ( $N \geq 3$ ) is shown. One-way ANOVA (DF = 3;  $P < 0.001$ ) was performed with Holm-Sidak post hoc test for each treatment group versus the control group (FLAG-HDA6 activity), \*\* $P \leq 0.01$ , \*\*\* $P \leq 0.001$ .

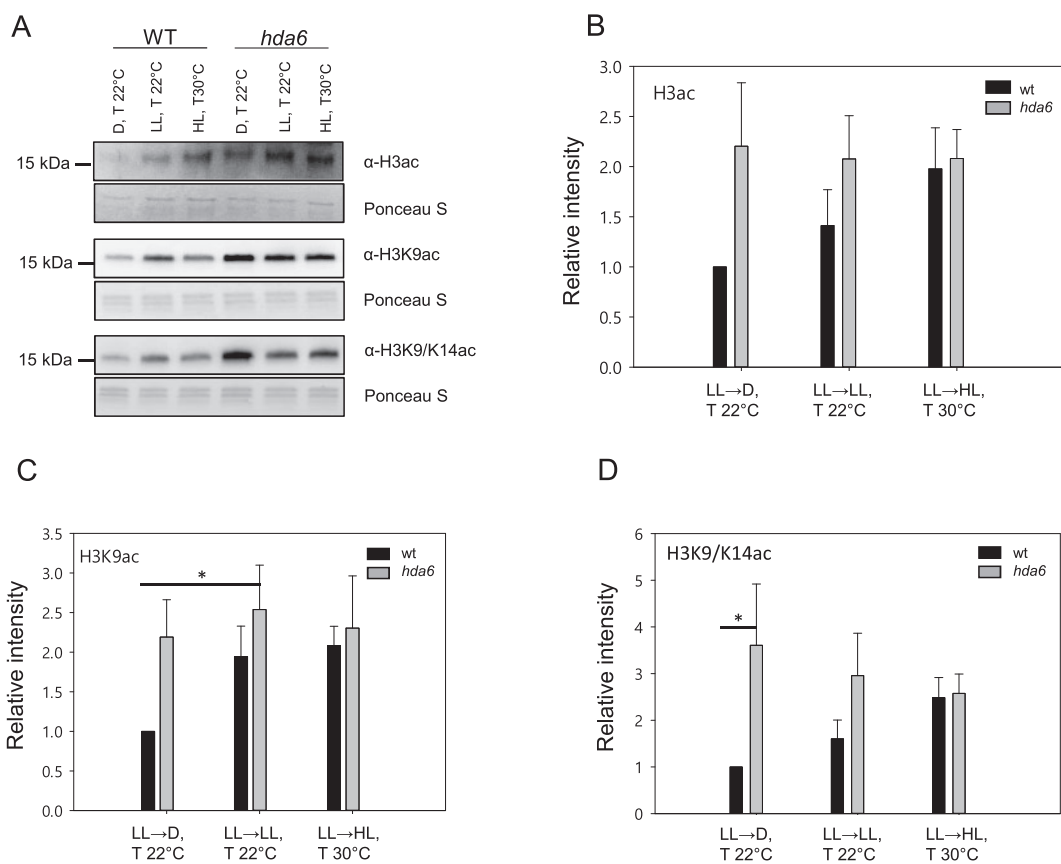


**Figure 4** Different light conditions lead to altered H3 acetylation in wt and *hda6* plants. **A**, Immunoblot detection of histone modifications. Four-week-old plants were exposed for 4 h to the indicated light conditions. Histones were extracted and analyzed for the indicated histone marks. **B–D**, Quantitative analysis of the immunodetected bands of the different histone marks. Signal intensity was determined with Image J software. Mean  $\pm$  se of at least three independent experiments ( $N \geq 3$ ) is shown. Intensities are given relative to the histone acetylation level in wt under D conditions, which was set to 1. Significant deviations from this constant were determined by Holm adjustment after one-way ANOVA (\* $P \leq 0.05$ ).

GSNOR and HDA6 activities, we performed ChIP-seq using an anti-H3K9ac antibody. H3K9ac is a hallmark of active gene promoters (Karmadiya et al., 2012) and this histone mark shows a trend towards higher abundance in *gsnor* (Figure 2C) and *hda6* (Figure 4C) mutants in comparison to wt, under both dark and LL conditions. Four-week-old wt, *gsnor*, and *hda6* plants were either exposed to low PPFD intensity or transferred to the dark for 4 h before a genome-wide light/dark-dependent H3K9ac profiling was performed by ChIP-seq. For all samples, the sequence reads aligned well with the *Arabidopsis* genome, resulting in a total of 95.31%–99.34% aligned reads (Supplemental Table S1). After peak calling (Zhang et al., 2008), quantification and differential analyses were performed to compare acetylation between light conditions and genotypes (Ross-Innes et al., 2012; Stark and Brown, 2019). Principle component analysis (PCA) based on all the peaks demonstrated a good clustering of replicates (Figure 5A). Principle component 1 shows light to dark effects for all genotypes (Figure 5A).

The highest density of H3K9ac peaks was found along the chromosome arms, whereas centromeric and pericentromeric regions were considerably less enriched in H3K9ac

(Figure 5B). The number of H3K9ac peaks was significantly increased in the *hda6* mutant compared to wt and *gsnor* (Figure 5, B and C). This hyperacetylation of DNA in *hda6* was observed throughout all chromosomes (Figure 5B). Most peaks were located 200–300-bp downstream of the closest transcription start site (TSS; Figure 5D). More than 93% of all peaks were found within 2-kb upstream or downstream of a TSS.

Most of the peak summits (~55%) are located within a coding sequence (CDS), and ~9% were observed in five-prime untranslated regions (5'-UTR) and 2-kb upstream regions (Figure 5E). In total, we identified 16,276 H3K9ac peaks. Differences in H3K9ac between LL and D conditions were identified for each genotype (e.g. wt LL versus wt D; adjusted  $P$ -value  $<0.05$ ). All plant lines exhibited light-dependent acetylation changes, with a positive effect preferentially on chloroplast and transport genes, and a negative effect preferentially on stress response and transcription genes (Figure 6A; Supplemental Tables S2 and S3). Peaks exclusively hyperacetylated or hypoacetylated in wt or both mutants could also provide hints to the functions of HDA6 and GSNOR in the context of light stimulus-dependent

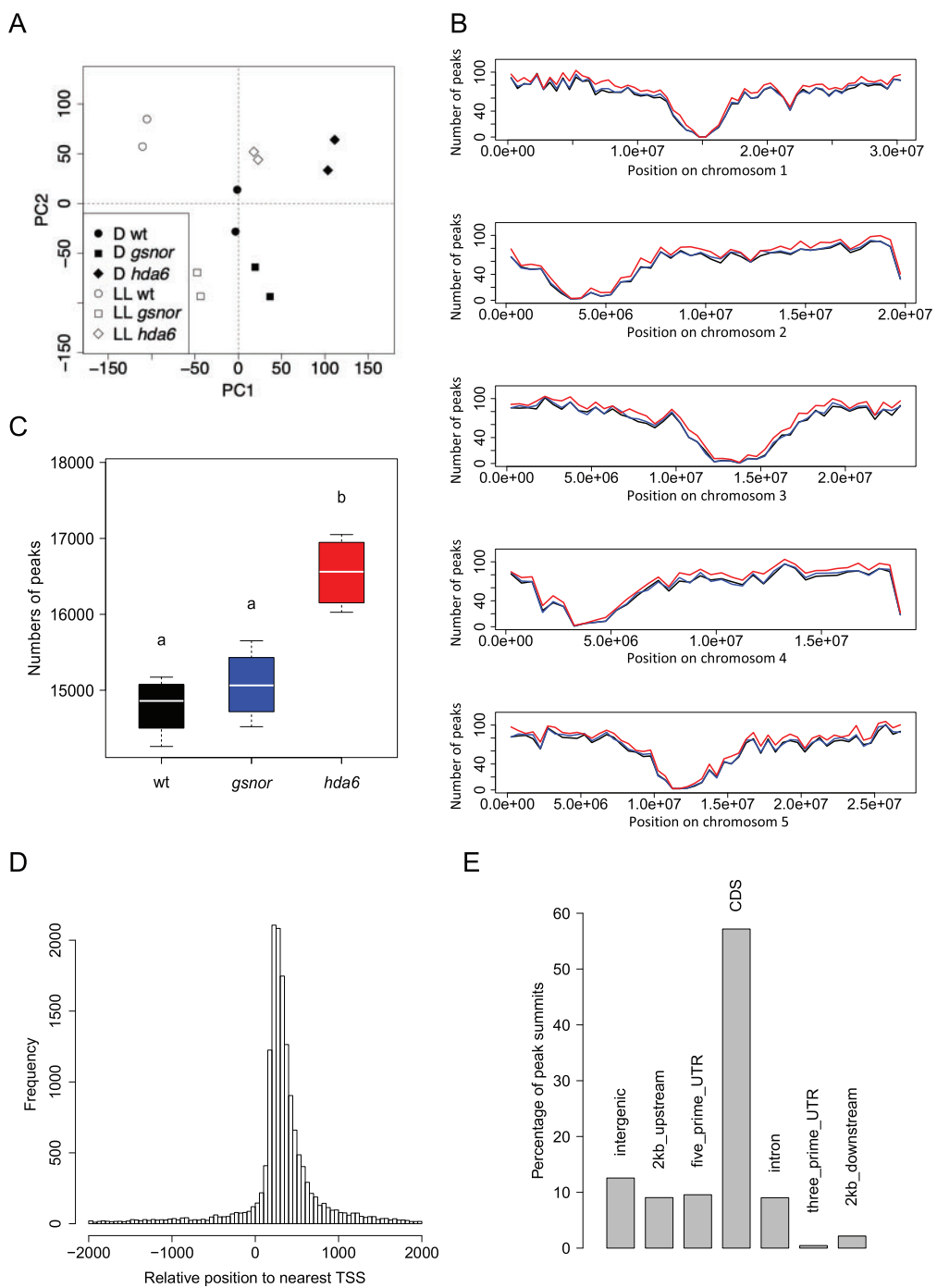


**Figure 5** Characteristics of ChIP-seq samples. **A**, PCA. The projection onto the top two principal components (30% and 27% of variance, respectively) shows a clustering of biological replicates. Two independent ChIP-seq experiments were performed ( $N = 2$ ). **B**, Chromosomal location of H3K9ac peaks averaged for each line. The number of peaks in each 500 kb chromosomal bin of the *Arabidopsis* genome is shown. The centromeric and pericentromeric regions of each chromosome are characterized by a very low number of peaks. Black: wt, blue: gsnor, red: hda6. **C**, total number of identified peaks for wt, gsnor, and hda6. Boxes show 25% and 75% quantiles, the white line represents the median, and the whiskers indicate the extreme values. Lower-case letters mark groups that are statistically different (Kruskal Wallis test with post hoc Dunn test,  $P < 0.05$ ). **D**, Location of H3K9ac peaks relative to genes. Histogram of distances of peak summits to the closest annotated TSS. The distribution shows a maximum at 200–300-bp downstream of the TSS. **E**, Distribution of H3K9ac peaks according to the genomic region of the summit (relative to the closest TSS). UTR, untranslated region.

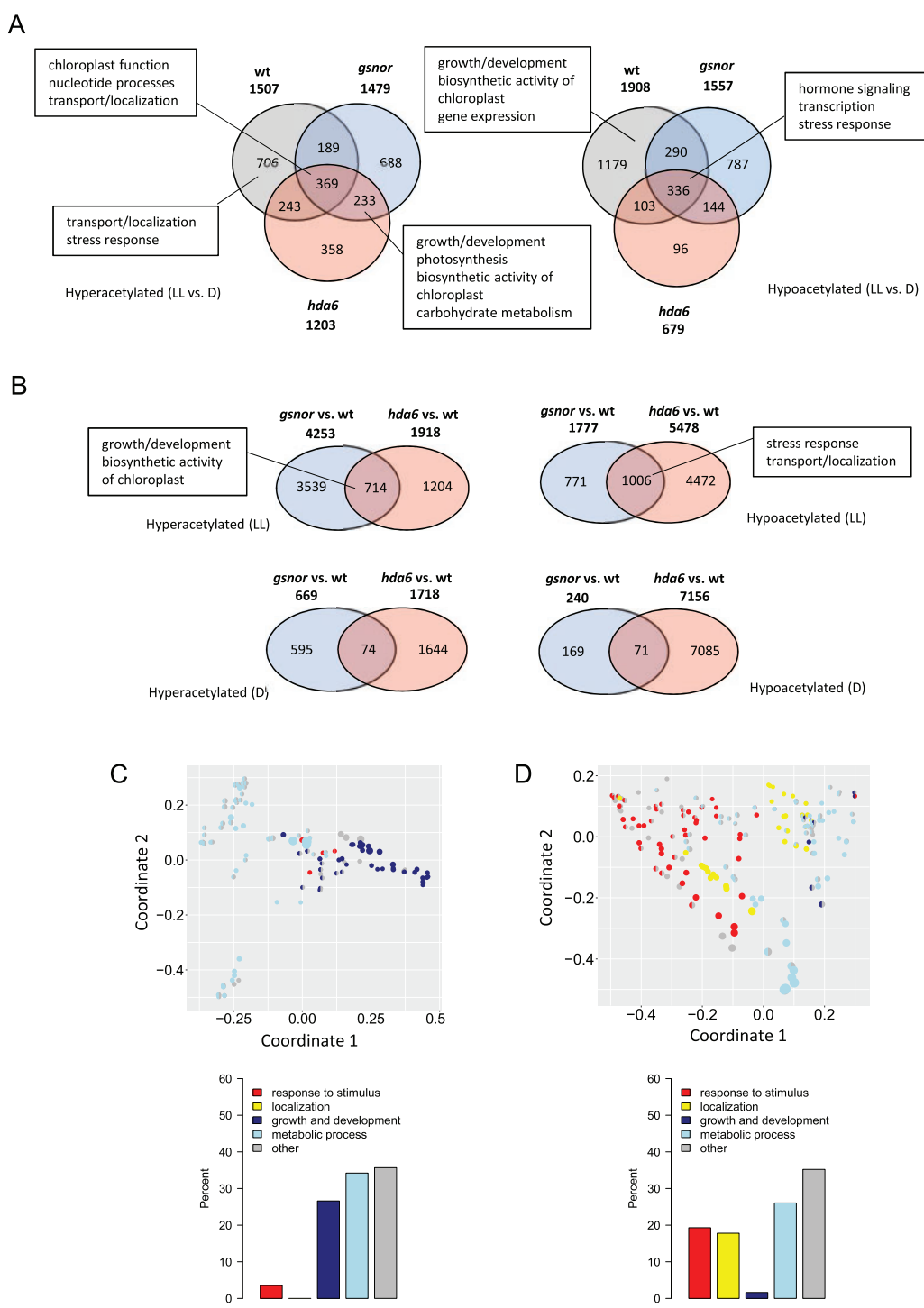


**Figure 6** Differential acetylation in mutants. A, B, Overlap of differentially acetylated peaks. Venn diagrams of significantly changed peaks (adjusted P-value < 0.05) in LL versus D (A) and mutants versus wt (B) comparisons. Boxes show major themes among significantly enriched GO terms (adjusted P-value < 0.05) for the respective partition. C and D, MDS analysis of significantly enriched GO terms (adjusted P-value < 0.05) among the genes with TSS closest to significantly upregulated or downregulated acetylation peaks (adjusted P-value < 0.05) that changed for both mutants versus wt under LL conditions. Only GO terms from the biological process ontology are shown in the plots. Each circle corresponds to an enriched GO term and circle size is proportional to the number of differentially acetylated genes (C: upregulated, D: downregulated) assigned to the GO term. The enriched GO terms are arranged in two dimensions such that their distance reflects approximately how distinct the corresponding sets of differential genes are from each other, that is, neighboring circles share a large fraction of genes. Each enriched GO term is colored by its membership in the top-level categories, which are grouped into five themes. If a GO term belongs to multiple top-level terms, a pie chart within the circle indicates the relative fraction of each theme. The total distribution of themes across all enriched GO terms is depicted in the bar plot underneath.

histone acetylation. The wt was characterized by a hyperacetylation of stress responsive genes and a hypoacetylation of growth/development and chloroplast genes, whereas the mutants showed a hyperacetylation of genes involved in growth/development, carbohydrate metabolism, and photosynthesis (Figure 6A; Supplemental Table S3).

### Under LL conditions, GSNOR and HDA6 regulate H3K9ac of genes involved in growth/development, stress response, and localization

Although the response to light already revealed differences between mutants and wt, a direct comparison of mutant and wt H3K9 acetylation under specific conditions will help to identify the basic functions of GSNOR and HDA6. H3K9ac peaks of *gsnor* and *hda6* were compared to H3K9ac peaks of wt plants under both LL and D conditions (e.g. *gsnor* LL versus wt LL). The number of hyperacetylated H3K9ac peaks is higher in *gsnor* than *hda6* plants (Figure 6B). Remarkably, six times more H3K9 loci are hyperacetylated in LL in comparison to D conditions for *gsnor* (Figure 6B). In the *hda6* mutant, more H3K9 marks were hypoacetylated in comparison to wt than in *gsnor* (Figure 6B). Interestingly, both mutant lines share many more specifically hyperacetylated and hypoacetylated peaks in LL conditions in comparison to D conditions. In total, 714 and 1,006 specifically hyperacetylated and hypoacetylated peaks, respectively, are shared under LL conditions, with highly significant *P*-values for the overlap (2.7e-30 and 1.5 e-98, respectively), whereas 74 and 71 shared hyperacetylated and hypoacetylated peaks, respectively, were found in D conditions (Figure 6B).

To examine, which biological functions are shared by GSNOR- and HDA6-specific changes in chromatin acetylation, a Gene Ontology (GO) term enrichment analysis was performed for the loci shared by both mutants. The corresponding genes of the hyperacetylated peaks (LL conditions) are enriched in GO terms, which mainly belong to growth/development (25%) and metabolic processes (>30%) including biosynthetic activity of chloroplasts, such as starch and pigment biosynthesis (Figure 6, B and C; Supplemental Table S4). The genes identified within the hypoacetylated peaks (LL conditions) are enriched in GO terms related to stress response (~20%), localization (~20%), and metabolic processes (~25%; Figure 6, B and D; Supplemental Table S4). In sum, these data suggest that GSNOR and HDA6 functions are required to deacetylate growth/development genes, in particular. Moreover, both enzyme functions promote acetylation of genes involved in stress response and localization.

### Transcript profiling of wt, *gsnor*, and *hda6* reveals gene regulation by light

As H3K9ac is often found in actively transcribed promotor and CDS, we performed RNA-seq using the same experimental setup used for the ChIP-seq experiment. In all three genotypes, around 6,000 genes are upregulated or

downregulated (adjusted *P*-value <0.05; Figure 7A; Supplemental Table S2). They share an overlap of 4,718 upregulated and 4,598 downregulated genes, which by design, are independent of GSNOR and HDA6 function, and are related to, for example, chloroplast and ribosome functions (Figure 7A; Supplemental Table S5). In contrast, the 580 and 578 genes that are exclusively upregulated and downregulated, respectively, in both mutants, depend on both enzyme functions. The upregulated genes act in processes related to growth/development and transport/localization, whereas the downregulated genes mainly function in stress response and transport/localization. Genes, that are exclusively upregulated in wt are enriched in GO terms predominately related to stress response (Figure 7A; Supplemental Table S5). This is consistent with the increased acetylation of stress response genes in wt (Figure 6A). Taken together, these results suggest a GSNOR- and HDA6-dependent induction of stress responsive genes and repression of growth/development genes in response to light.

To identify common regulatory functions of GSNOR and HDA6 activities in gene expression, the transcriptomes of *gsnor* and *hda6* were directly compared to wt, both under LL and D conditions. Similar to the acetylation data, in both genotypes, more genes are differentially regulated under LL conditions than under D conditions (Figure 7B). Notably, the GO term enrichment results for the LL conditions share some overall trends with the ChIP-seq data (Figure 7, C and D; Supplemental Table S6). While stress response functions are overrepresented among the genes downregulated in both mutants, growth/development functions are only prominent among the upregulated genes of both mutants. Different from the ChIP-seq results, many genes with transport/localization functions are upregulated in both mutants.

### Coregulation between H3K9ac and gene expression in *gsnor* and *hda6* under LL conditions

To analyze the influence of H3K9ac on gene expression, ChIP-seq and RNA-seq datasets were integrated at the gene level for both mutants. Under LL conditions, the two mutants share 23 genes that show hyperacetylation and enhanced expression in comparison to wt plants (Table 1; Supplemental Table S7). Interestingly, this group contains genes involved in growth/development, for example, brassinosteroid biosynthesis (cytochrome P450 superfamily protein, AT3G50660), cell wall formation (glycosyl hydrolase family protein, AT1G78060), auxin biosynthesis (tryptophan aminotransferase related 2, AT4G24670), serine biosynthesis (D-3-phosphoglycerate dehydrogenase, AT4G34200), and histone modification (histone-lysine N-methyltransferase SETD1B-like protein, AT5G03670; Figure 8; Supplemental Table S2). Under D conditions, only three genes are hyperacetylated and overexpressed in both mutants. One of these genes, AT5G16980 (Zinc-binding dehydrogenase family protein), has also shown up

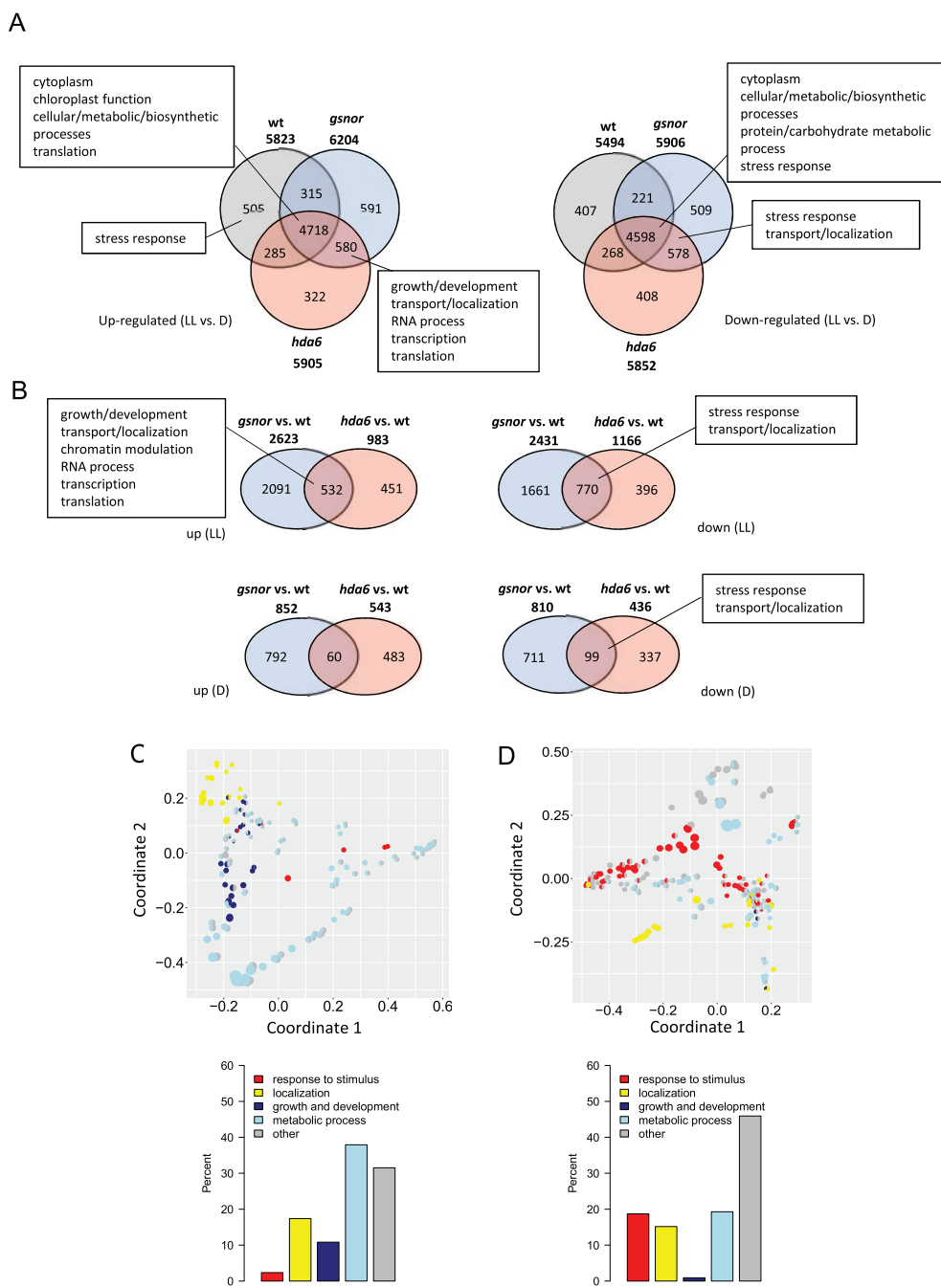


**Figure 7** Differential gene regulation in mutants. A and B, Overlap of differentially expressed genes. Venn diagrams of significantly changed genes (adjusted  $P$ -value  $< 0.05$ ) in LL versus D (A) and mutants versus wt (B) comparisons. C and D, MDS analysis of enriched GO terms (adjusted  $P$ -value  $< 0.05$ ) among the significantly upregulated or downregulated genes (adjusted  $P$ -value  $< 0.05$ ) changed for both mutants versus wt under LL conditions. Only GO terms from the biological process ontology are shown in the plots. Each circle corresponds to an enriched GO term and circle size is proportional to the number of differentially regulated genes assigned (C: upregulated, D: downregulated) to the GO term. See Figure 6 for further details about the plots.

under LL conditions and is putatively involved in redox processes in plastids and cytosol.

In addition, 65 genes are hypoacetylated and less expressed in both mutants under LL conditions (Table 1; Supplemental Table S8). These include several genes involved in abiotic and biotic stress response, for example,

RNA-binding KH domain-containing protein (AT1G14170), calcium-dependent protein kinase 2 (AT1G35670), protein kinase superfamily protein (AT1G53165), trehalose-phosphatase/synthase 9 (AT1G23870), aminophospholipid ATPase 1 (AT5G04930), oxidative stress 3 (AT5G56550), GRIP/coiled-coil protein (AT3G14430), and bZIP transcription

**Table 1** Selected genes showing corresponding H3K9ac and gene expression

ATG	Gene	Function (according to TAIR database)
Mutant effect LL_down GO:0050896 Response to stimulus/GO:0006950 Response to stress/GO:0009628 Response to abiotic stimulus		
AT1G23870	Trehalose-phosphatase/synthase 9	Trehalose biosynthesis.
AT3G14430	GRIP/coiled-coil protein	Response to oxidative stress.
AT5G56550	Oxidative stress 3	Response to cadmium ion, response to oxidative stress.
AT5G04930	Aminophospholipid ATPase 1	Lipid flippases promote antiviral silencing and the biogenesis of viral and host siRNAs in Arabidopsis.
AT5G28770	bZIP transcription factor family protein	The Arabidopsis bZIP gene AtbZIP63 is a sensitive integrator of transient ABA and glucose signals.
AT1G53165	Protein kinase superfamily protein	Hyperosmotic response, response to salt stress, response to wounding.
Mutant effect LL_up GO:0040007 Growth/GO:0048856 Anatomical structure development		
AT1G78060	Glycosyl hydrolase family protein	Arabinan and xylan catabolic process.
AT4G24670	Tryptophan aminotransferase related 2	TAR2 is required for reprogramming root architecture in response to low nitrogen conditions.
AT4G34200	D-3-phosphoglycerate dehydrogenase	Brassinosteroid biosynthetic pathway.
AT3G50660	Cytochrome P450 superfamily protein	
AT5G03670	Histone-lysine N-methyltransferase SETD1B-like protein	Histone methyltransferase that specifically methylates H3K4.

ChIP-seq and RNA-seq datasets were integrated at the gene level for both mutants to analyze the effect of H3K9ac on gene expression. Genes downregulated and upregulated in both mutants under LL conditions are shown. Protein functions are given according to the TAIR database.

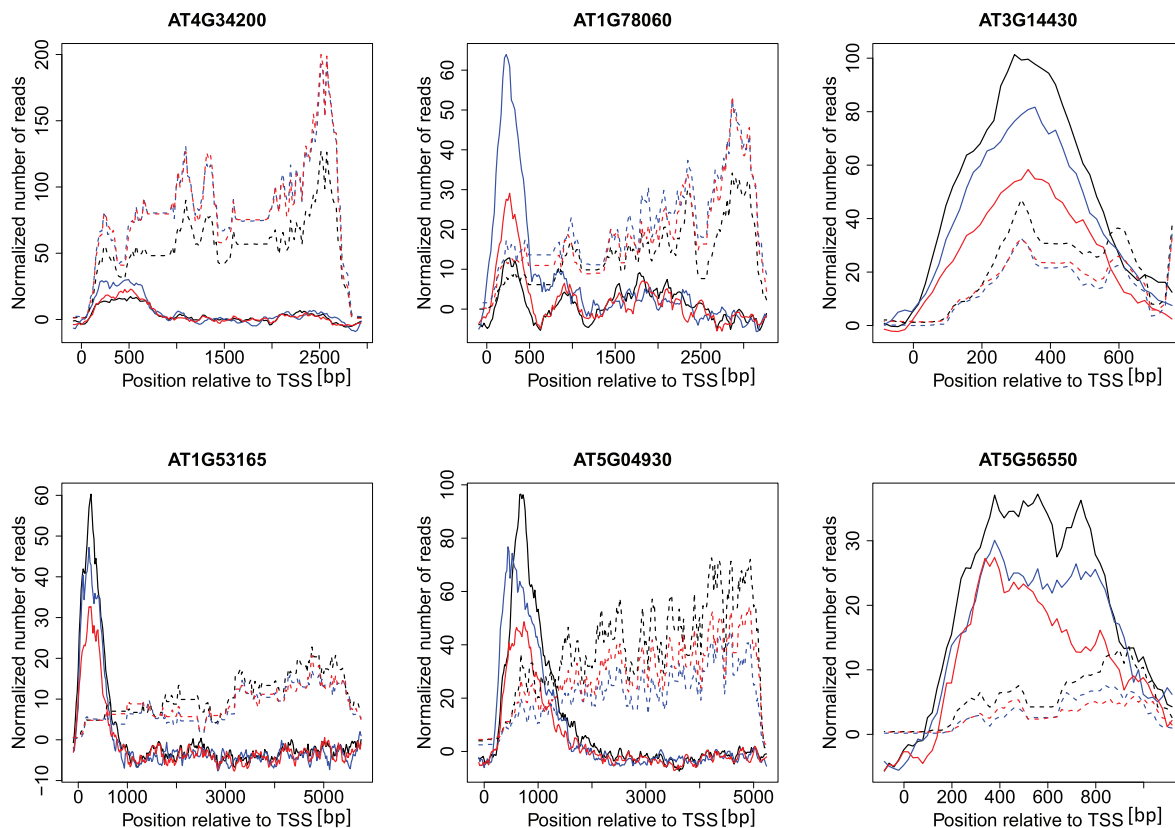


**Figure 8** Gene level integration of ChIP-seq and RNA-seq datasets for both mutants under LL conditions. Comparative visualization of H3K9ac and gene expression. ChIP-seq (solid lines) and RNA-seq (dashed lines) results of selected genes involved in growth/development (AT4G34200: D-3-phosphoglycerate dehydrogenase, AT1G78060: Glycosyl hydrolase family protein) and stress response (AT3G14430: GRIP/coiled-coil protein, AT1G53165: Protein kinase superfamily protein, AT5G04930: Aminophospholipid ATPase 1, AT5G56550: oxidative stress 3) are shown. Wt: black, gsnor: blue, hda6: red.

factor family protein (AT5G28770; **Figure 8**; Supplemental Table S2).

## Discussion

### Increasing light intensity enhances SNO accumulation and NO emission

NO is an important signaling molecule that is involved in transcriptional regulation of many different physiological processes in plants related to growth and development, abiotic and biotic stress response, and photosynthesis (Huang et al., 2002; Polverari et al., 2003; Parani et al., 2004; Kovacs et al., 2016; Kuruthukulangarakoola et al., 2017). We observed an emission/accumulation of NO/SNO in the dark, and which increased in light phases (**Figure 1**). GSNOR is responsible for controlling SNO homeostasis, and loss of GSNOR function results in enhanced levels of SNO (**Figure 1, B, E–G**). A similar observation was reported by other groups who demonstrated that endogenous NO production in *Arabidopsis* leaves exhibits a diurnal rhythm where the NO level was reduced by 30% at night (He et al., 2004). Moreover, light-dependent NO release has been reported for tobacco leaves (Planchet et al., 2005). This indicates that light is an important trigger for intracellular accumulation of NO/SNO. NO production and emission under light conditions could be based on light-triggered activation of nitrate reductase activity (Riens and Heldt, 1992; Rockel et al., 2002; Planchet et al., 2005). However, since the NO emission of nitrite reductase (NiR)-deficient tobacco leaves still increased in light, other factors besides these reductase activities might also contribute to NO production (Planchet et al., 2005). For example, it could be that reduction of  $\text{NO}_2^-$  to NO is related to photosynthetic electron flux where ferredoxin functions as an electron donor. Reduction of  $\text{NO}_2^-$  to NO is also possible in mitochondria of plants and animals in the presence of NADH (Kozlov et al., 1999; Stoimenova et al., 2007). However, this reaction is only observed under low oxygen conditions (Gupta et al., 2010). NO production in mammals corresponds to the light-triggered expression and activity of NOS (Ko et al., 2013; Machado-Nils et al., 2013). Although NOS enzymes have not been found in higher plants yet, it was demonstrated that NO can be produced in the chloroplast via an NADPH-dependent oxidation of L-arginine, which is the substrate of NOS. It has been shown that L-arginine is one the most common amino acids in chloroplasts and available there in nanomolar concentrations (Jasid et al., 2006). The synthesis of L-arginine is controlled by the photosynthetic light reaction, suggesting that oxidative NO production might also follow a circadian-like pattern. Stomata are usually open during the day (light) and closed at night (darkness), which might affect NO emission from leaves. However, light-dependent accumulation of endogenous SNOs and nitrite (**Figure 1, E–G**) excluded the possibility that the observed light-dependent NO emission is only due to light-regulated stomata opening. In sum, the observed light-dependent NO/SNO accumulation/emission suggests a

signaling function of this redox molecule in light-regulated processes. Moreover, as *gsnor* mutants showed increased NO emission and SNO accumulation under light (**Figure 1, B, E–G**), *in vivo* GSNOR activity seems to have a regulatory function in light-dependent NO/SNO homeostasis.

### Light-induced NO/SNO accumulation corresponds to histone acetylation

In addition to the direct modification of metabolic pathways and regulation of gene expression, NO can target the modulation of the chromatin structure, which is a less investigated regulatory mechanism. We observed a positive association between light intensity, NO/SNO accumulation, and histone acetylation. The higher the light intensity, the higher the amount of accumulated SNO (and released NO), and the higher the levels of global H3ac, H3K9ac, and H3K9/14ac in wt plants (**Figures 1, 2**). Such an association was not observed in *gsnor* plants (**Figure 2**), suggesting a regulatory function of GSNOR activity (lower SNO level, denitrosation) in histone acetylation under these conditions.

There are several pieces of evidence indicating that SNO-induced histone acetylation is a result of the inhibition of HDA activity. First, 500  $\mu\text{M}$  GSNO and SNAP reversibly reduced total HDAs activity by about 20% in protoplasts and nuclear extracts (Mengel et al., 2017). Second, stimulation of endogenous NO production also inhibits the catalytic HDA activity in protoplasts (Mengel et al., 2017). Third, there are hints that the activity of at least some HDA isoforms is redox-regulated. Redox-sensitive Cys residues have been described for *Arabidopsis* HDA9 and HDA19. It is suggested that the oxidation of these two HDAs promotes their deactivation and therefore enhances histone acetylation and enables expression of associated genes (Liu et al., 2015). Redox regulation of HDAs has already been described in animals and humans. For example, brain-derived neurotropic factor causes NO synthesis and S-nitrosation of human HDA2 at Cys262 and Cys274 in neurons. However, in this mammalian system, S-nitrosation of HDA2 does not inhibit deacetylase activity, but causes its release from a CREB-regulated gene promoter. Oxidation of HDA2 results in enhanced H3 and H4 acetylation at neurotrophin-dependent promoter regions and facilitates transcription of many genes (Nott et al., 2008). A different study reported about S-nitrosation of HDA2 in muscle cells of dystrophin-deficient MDX mice (Colussi et al., 2008). Although NO-sensitive Cys of this enzyme are not identified yet, it was shown that the enzymatic activity of muscle HDA2 is impaired upon treatment with the NO donor DETA-NO. Furthermore, recombinant mammalian HDA6 and HDA8 have been reported to undergo S-nitrosation resulting in inhibition of their catalytic activities (Feng et al., 2011; Okuda et al., 2015). Moreover, HDA4 and HDA5, as parts of a large protein complex, migrate into the nucleus upon S-nitrosation of protein phosphatase 2A (Illi et al., 2008). Based on the studies mentioned above,

mammalian HDAs seem to play an important role in redox-signaling (1) directly via NO or ROS production or (2) indirectly by impairing HDA activities.

Similar mechanisms seem to be present in plants. Interestingly, Arabidopsis HDA6 shares ~60% amino acid sequence identity with mammal HDA2, which is redox-sensitive (Figure 3A). Both proteins contain seven Cys residues, which are located within the HDA domain. NO/SNO-sensitive Cys residues of human HDA2 are conserved in Arabidopsis HDA6 and are located at similar positions in the 3D structure of the proteins. The catalytic activity of purified in planta-produced FLAG-HDA6 is partially inhibited by GSNO (Figure 3, E and F). Since S-nitrosation of HDA6 could be detected using the biotin switch assay, NO-mediated inhibition of HDA6 activity could be caused by PTM of cysteine residues. Surprisingly, the activity of GSNO-treated FLAG-HDA6 could not be restored by subsequent treatment with 5 mM DTT. In contrast, addition of DTT further inhibited HDA6 activity by 30%. Likely, these quite strong reducing conditions resulted in loss of complex partners important for HDA6 activity or caused structural changes of the HDA6 protein.

H3ac, H3K9ac, and H3K9/14ac levels tend to be higher in *hda6* plants in D conditions in comparison to wt plants (Figure 4, B–D), while under HL conditions, the acetylation levels of the *hda6* mutant and wt are similar. Interestingly, HDA6 controls light-induced chromatin compaction in Arabidopsis (Tessadori et al., 2009). The *hda6* mutant displayed a substantially lower heterochromatin index under LL intensities ( $<400 \mu\text{mol m}^{-2} \text{s}^{-1}$ ) than the corresponding wt plants. However, at HL intensities ( $>500 \mu\text{mol m}^{-2} \text{s}^{-1}$ ) the heterochromatin index increased drastically in *hda6*, indicating a regulatory function of HDA6 in light-induced chromatin compaction (Tessadori et al., 2009). As low- and high-histone acetylation levels correspond to compact and loose chromatin structure, respectively, our data confirm that HDA6 is involved in light-dependent chromatin modulation and imply HDA6 is a promising candidate for a NO-affected HDA isoform. The proposed mechanism for the deacetylating function of GSNOR and HDA6 in D conditions is shown in Figure 9.

### Genome-wide profiling of H3K9ac in wt, *gsnor*, and *hda6* shows enrichment close to TSSs

ChIP-seq analysis on H3K9ac was performed to examine the functions of GSNOR and HDA6 on chromatin structure in the dark and under light conditions; 16,276 H3K9ac sites were found in the chromatin of Arabidopsis leaf tissue. Peaks mainly resided within gene-enriched areas and were almost depleted from centromeric and pericentromeric regions (Figure 5B). This observation is in line with reports from other plant species or other histone acetylation marks. For example, in the moss *Physcomitrium patens*, H3K9ac and H3K27ac, and in rice, H3K9ac, showed a strong enrichment in genic regions (He et al., 2010; Widiez et al., 2014).

The genome-wide profiling of H3K9ac in Arabidopsis revealed that this histone modification is predominantly located within the regions surrounding the TSSs of genes, with a maximum at 200–300-bp downstream of the TSS (Figure 5D). This agrees with the distribution of H3K9ac in other plants as well as the distribution of other histone marks, for example, analysis of different histone modification profiles in Arabidopsis revealed that most peaks are localized around 480-bp downstream of the TSSs, whereas peak position, shape, and length are independent of gene length (Mahrez et al., 2016; Ayyappan et al., 2019). Moreover, the preferential binding of transcription factors (~86%) between –1,000 and +200 bp from a TSS has been found in Arabidopsis (Yu et al., 2016). The *hda6* mutant displayed more acetylated regions than wt and *gsnor* throughout all chromosomes (Figure 5, B and C).

### GSNOR and HDA6 coordinate H3K9ac of genes involved in chloroplast function and growth/development

GO term analysis revealed that, under light conditions, *gsnor* and *hda6* share hyperacetylated genes related to chloroplast activity and growth/development (Figure 6, A–C). These data suggest that GSNOR and HDA6 function is required to deacetylate these genes under light conditions. Many plants produce and store metabolites and energy during the day, which are used for growth/development during the night (Graf et al., 2010; Apelt et al., 2017). From this point of view, it makes sense that acetylation of genes involved in growth/development is reduced in the light, making these genes less accessible for the transcription machinery, whereas acetylation in the dark enables their transcription. Genes related to chloroplast function mainly relate to starch, sulfur and terpenoid metabolism. As the products of these genes are also required under light conditions, their reduced acetylation is surprising. However, since the acetylation levels of histones are the result of a fine-tuned interplay between acetyltransferases and HDAs, GSNOR and HDA6 are probably required to keep a balanced acetylation level of these genes. That is in line with the observation that expression of this set of genes does not change substantially in both mutants in comparison wt.

The regulatory mechanisms of the deacetylating function of GSNOR under light are unknown. GSNOR activity lowers the level of GSNO and consequently lowers the level of S-nitrosated proteins. In this way, GSNOR is protecting HDA6 from SNO-dependent inhibition and keeping it active (Figure 9). However, our data do not rule out additional effects of NO, for example, activation of other HDAs or a reduced activity of distinct histone acetyltransferases. To get insight into the regulatory function of SNOs in chromatin modulation during light–dark switch, the S-nitrosylome under these conditions needs to be identified. In conclusion, according to the results obtained with the *gsnor* and *hda6*

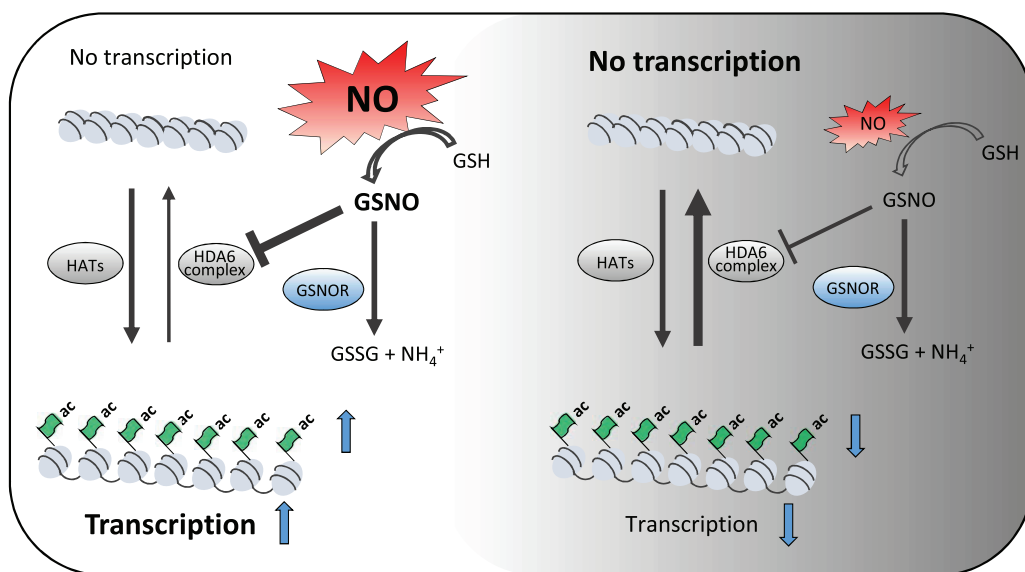


**Figure 9** Schematic illustration of the regulatory function of NO on histone acetylation in light and dark conditions. Light-induced production of NO/GSNO results in enhanced inhibition of HDA6, and increases histone acetylation gene transcription (left side). In dark conditions, HDA6 activity is enhanced because of less NO/GSNO production. As a consequence, histone acetylation and gene transcription are decreased. In both situations, GSNOR activity is required for fine-tuning the SNO levels.

genotypes, both enzymes seem to play an important role in the light-dark (diurnal) regulation of histone acetylation.

#### GSNOR and HDA6 regulate H3K9 deacetylation and repression of genes involved in plant growth/development

Under light conditions, both mutants share several genes involved in growth/development, which show hyperacetylation and enhanced expression in comparison to wt plants, for instance histone-lysine N-methyltransferase SET DOMAIN CONTAINING 1B (SETD1B)-like protein (AT5G03670). In *Arabidopsis*, 12 SET DOMAIN GROUP (SDG)-containing histone methyltransferases are present, which are mainly involved in H3K4 and H3K36 methylation. These marks are marks of active transcription. So far, only a few genes of this gene family have been functionally characterized. SDG25, for instance, is involved in FLOWERING LOCUS C (FLC) activation and repression of flowering (Berr et al., 2009). FLC is a key regulator of flowering, which negatively regulates downstream flowering activators such as PUTATIVE FLOWERING SIGNALS MEDIATING PROTEIN FT and SUPPRESSOR OF OVEREXPRESSION OF CO1 (Helliwell et al., 2006). Consequently, high expression of FLC results in a late-flowering phenotype. Interestingly, in both *gsnor* and *hda6* mutants, histone-lysine N-methyltransferase SETD1B-like protein acetylation and expression were increased, and both mutants displayed a late-flowering phenotype (Wu et al., 2008; Yu et al., 2011; Kwon et al., 2012), indicating a flowering-activating role of GSNOR and HDA6. In *hda6*, the late-flowering phenotype is likely due to upregulation of FLC expression (Yu et al., 2011; Supplemental Table S6). In contrast, for *gsnor*, reduced or unchanged expression of

FLC in comparison to wt plants is reported (Kwon et al., 2012; Supplemental Table S6), suggesting that GSNOR and HDA6 have different functions in regulating flowering time.

Besides regulating the flowering time, GSNOR and HDA6 also seem to have important common regulatory functions in brassinosteroid biosynthesis. The gene encoding the cytochrome P450 superfamily protein (AT3G50660; DWARF4) was hyperacetylated and more highly expressed in both mutants in comparison to wt plants. DWARF4 encodes a 22 $\alpha$  hydroxylase that catalyzes a rate-limiting step in brassinosteroid biosynthesis (Choe et al., 2001). Brassinosteroids are phytohormones important for plant growth and development as well as for response to environmental stress. Mutants in the brassinosteroid pathway often display a dwarf phenotype (Li et al., 2001; Kim et al., 2013). Interestingly, *gsnor* displays a dwarf phenotype (Holzmeister et al., 2011; Kwon et al., 2012), although the key gene of brassinosteroid biosynthesis is upregulated, indicating that enhanced brassinosteroid biosynthesis is probably counteracting the dwarf phenotype that resulted from GSNOR knockout. In sum, our results demonstrate that GSNOR and HDA6 are playing a role in negatively regulating histone acetylation and expression of genes involved in growth/development and chloroplast function.

#### GSNOR and HDA6 promote H3K9ac and expression of genes involved in plant stress response

Metabolic reprogramming in response to abiotic and biotic stress is governed by a complex network of genes, which are induced or repressed. A large set of stress-related genes is exclusively hyperacetylated in wt under LL versus D

conditions (Figure 6A). Light dependency of plant stress response has been investigated in the past in different contexts, for example, circadian rhythm, day/night length, and light composition (Griebel and Zeier, 2008; Sano et al., 2014; Grundy et al., 2015; D'Amico-Damiao and Carvalho, 2018). Various reports have shown that the plant signaling pathways involved in the responses to abiotic and biotic stresses are modulated by different types of photoreceptors, controlling expression of a large fraction of abiotic stress-responsive genes as well as biosynthesis and signaling downstream of stress response hormones (Jeong et al., 2010; Ballare, 2014; Mazza and Ballare, 2015). For example, pathogen inoculations in the morning and midday resulted in higher accumulation of salicylic acid, faster expression of pathogenesis-related genes, and a more pronounced hypersensitive response than inoculations in the evening or at night (Griebel and Zeier, 2008). The observed plant defense capability upon daytime treatments seems to be attributable to the availability of a long light period during early plant-pathogen interaction rather than to the circadian rhythm. One might speculate whether, for example, the light-dependent flagellin 22-induced accumulation of salicylic acid (Sano et al., 2014) is related to H3K9ac. We observed light-dependent enrichment of the H3K9ac mark in many stress-related genes in wt in LL versus D comparison (Figure 6A). As H3K9ac is an activating histone mark, these genes might be prepared for expression, and according to the RNA-seq data, many stress-related genes display a higher expression in wt under light in comparison to darkness (Figure 7A).

Interestingly, GSNOR, as well as HDA6 function, seems to be involved in regulation of H3K9ac and expression of stress-related genes. Loss of GSNOR and HDA6 activity resulted in relative hypoacetylation and reduced expression of many stress-related genes (Figure 6, B and D), suggesting that both enzymes are required to activate these stress-related genes. Given its HDA function, this means that those stress genes are specifically not targeted by HDA6. The loss of a distinct HDA function could result in activation of other HDAs or reduction of histone acetyltransferase activities, but this is not shown by our data (Figure 4). Rather, the increased overall number of acetylated regions might decrease the acetylation intensity at certain sites. Moreover, other still unknown factors could be involved in regulating histone acetylation. Indeed, indirect gene activating function has also been observed for other HDAs, for example, for HDA5 (Luo et al., 2015), HDA9 (van der Woude et al., 2019), and HD2B (Latrasse et al., 2017).

Stress-responsive genes, which are hypoacetylated and downregulated under light conditions in both mutants, include OXIDATIVE STRESS 3 (ATSG56550; OXS3). OXS3 is a chromatin-associated factor involved in heavy metal and oxidative stress tolerance (Blanvillain et al., 2009). It contains a domain corresponding to a putative N-acetyltransferase or thioltransferase catalytic site. Enhanced stress tolerance of OXS3 overexpression lines and stress-sensitivity of oxs3 mutant indicates a role in stress tolerance. The nuclear

localization of this protein supports a function as stress-related chromatin modifier protecting the DNA or altering transcription (Blanvillain et al., 2009).

Interestingly, acetylation and expression of trehalose-phosphatase/synthase 9 is also reduced in *gsnor* and *hda6* plants. Trehalose is a disaccharide composed of two glucose bound by an alpha-alpha (1-1) linkage and is often associated with stress-resistance in a wide range of organisms (Fernandez et al., 2010). Trehalose accumulation has been observed in plants under different stress situations, such as drought, heat, chilling, salinity, and pathogen attack (Fernandez et al., 2010). Moreover, genes involved in detoxification and stress response are induced by exogenous application of trehalose (Bae et al., 2005a, 2005b; Govind et al., 2016) or by activating trehalose biosynthesis (Avonce et al., 2004).

The bZIP transcription factor family protein encodes for AtbZIP63, which is an important node of the glucose-abscisic acid (ABA) interaction network and may participate in the fine-tuning of ABA-mediated abiotic stress responses (Matiolli et al., 2011). The ABA signaling pathway is a key pathway that controls response to environmental stress.

Emission of NO and SNO level was higher under light compared to darkness (Figure 1, B, C, E–G). Although GSNOR inhibits the activity of recombinant HDA6 (Figure 3, E and F), their effects on stress-related genes are probably indirect. In addition, other HDAs and histone acetyltransferases can be involved in regulation of histone acetylation at stress-responsive genes. It was demonstrated that HDA19 plays an essential role in suppressing SA-biosynthetic genes and PR-genes during unchallenged conditions via deacetylating the corresponding promoters (Choi et al., 2012). After pathogen attack, histone acetylation at these regions increased, suggesting a reduction of HDA19 activity or alternatively, an activation/recruitment of histone acetyltransferase activity. Furthermore, in *Arabidopsis*, the plant-specific HD2B binds to genes involved in defense response in untreated plants, whereas after flg22 treatment, it is mainly genes involved in plastid organization that are targeted by HD2B (Latrasse et al., 2017).

All these observations highlight the importance of a fine-tuned switch between growth and development on one side and stress response on the other side. In this context, GSNOR and HDA6 play key roles coordinating histone acetylation and expression of stress-related genes and genes involved in growth/development to reduce plant growth/development and thereby allow a successful stress response (Figure 10). On the other side, the coordinating function of these enzymes and NO could be a promising target to modify plant metabolism to mitigate the negative effects of a stressful environment on plant performance and productivity. Moreover, our study shows that, in addition to the known suppressive effects of HDAs, HDA6 has indirect positive effects on transcription and interestingly, GSNOR activity seems to be involved in this process of switching the metabolism from growth and development to stress

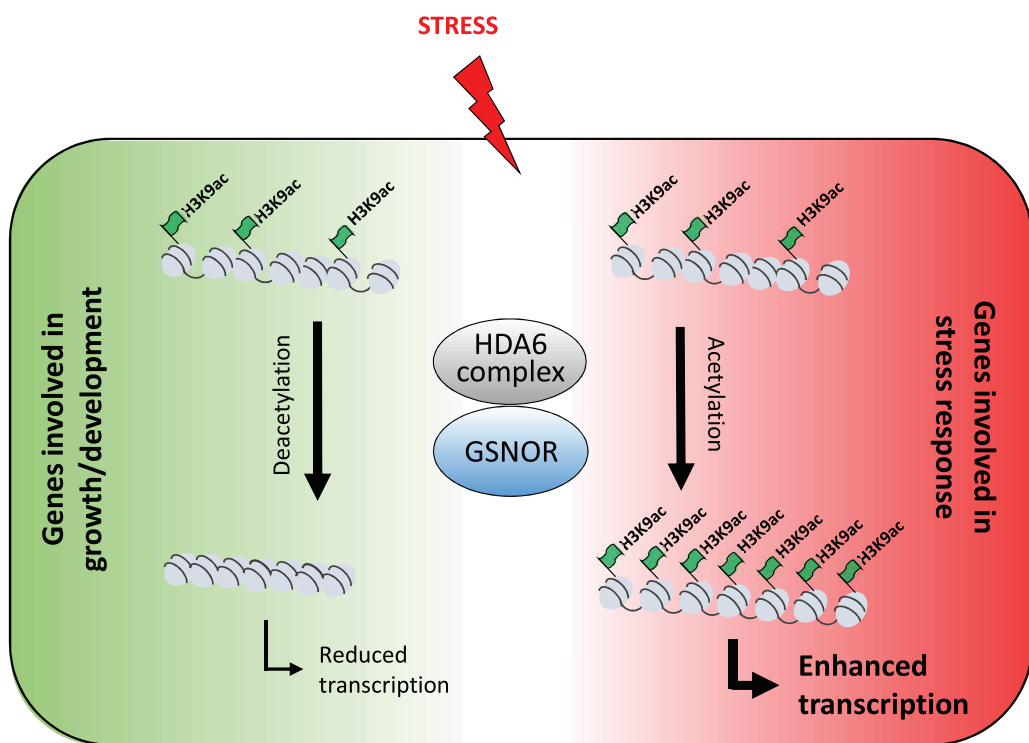


**Figure 10** Under stress conditions GSNOR and HDA6 differentially modulate H3K9ac of genes involved in growth/development and stress response. The model illustrates that GSNOR and HDA6 act in similar pathways responsible for regulating an identical set of growth/development-related genes as well as stress-related genes. Although GSNOR and HDA6 function is required for deacetylation and repression of genes involved in growth/development, both enzymes are also involved in acetylation and enhanced expression of stress-responsive genes, suggesting that GSNOR and HDA6 function as molecular switches between both physiological processes.

response. In sum, it appears that NO coordinates histone acetylation and expression of genes involved in growth/development and stress response.

## Materials and methods

### Plant lines, cultivation

*A. thaliana* wt Col-0, *gsnor1-3* (also called GABI-Kat 315D11, *gsnor*, or *GSNOR-KO*), *axe1-5* (also called *hda6* or *HDA6-ko*) were cultivated on soil mixed in 5:1 ratio with sand. The *hda6/axe1-5* allele used to generate the cell culture contains an insertion resulting in a premature stop codon and the expression of a nonfunctional, C-terminally truncated version of HDA6 (Murfett et al., 2001). Plants were grown under short day conditions (10-h light/14-h dark and 20°C/16°C, respectively). The relative humidity during the day and night was 50%. Light intensity was ~100–130 μmol photons m<sup>-2</sup> s<sup>-1</sup> PPFD. For treatment with different light conditions 4-week-old plants were transferred at 11 am for 4 h to dark (D, PPFD of 0 μmol photons m<sup>-2</sup> s<sup>-1</sup>, T 22°C), LL (PPFD of 200 μmol photons m<sup>-2</sup> s<sup>-1</sup>, T 22°C), or HL (PPFD of 1,000 μmol photons m<sup>-2</sup> s<sup>-1</sup>, T 30°C).

### Extraction of nuclear proteins

Nuclear proteins were extracted from *Arabidopsis* cell culture or seedlings according to the protocol of (Xu and

Copeland, 2012) with small modifications. Approximately 0.5–0.6 g of ground *Arabidopsis* tissue or cell culture was homogenized in 3 mL of LB buffer and sequentially filtered through two layers of miracloth and then 40-μm nylon mesh. The homogenate was centrifuged for 10 min at 1,500g and 4°C. The supernatant was discarded, and the pellet was resuspended in 3 mL of NRBT buffer and centrifuged as described above. This step was repeated two more times or until the green color (chloroplast contamination) was gone. Triton X-100 was removed from the nuclei pellet by washing in 3 mL of NRB buffer. If the nuclei were not used immediately, they were resuspended in 400 μL of NSB buffer, frozen in liquid nitrogen and stored at –80°C.

Two methods were used to break a nuclear envelope and solubilize proteins. For quick detection of nuclear proteins by western blot, the nuclear pellet was resuspended in 50 μL of Laemmli buffer, heated for ~10 min at 95°C and centrifuged for 15 min at 20,000g. Protein concentration was measured using a RC DC protein assay (Biorad, Cat No. 5000121). The second method was based on the sonication procedure using microtip MS 72 (Bandelin, Cat No. 492). The nuclei pellet was resuspended in ~300 μL of NPLB buffer and sonicated for 30 s, with the settings step 3 and 20%–40%. The sonication step was repeated in total five times with ~1 min break in between. Protein concentration

was measured using a Bradford reagent (Biorad, Cat No. 5000006).

### cPTIO treatment of *Arabidopsis* plants

Four- to five-week-old *Arabidopsis* wt plants grown on soil under short-day conditions (10/14 h light/dark, 20/17°C) were sprayed with 200 µM of cPTIO (in 0.002% (w/v) Tween 20) and transferred for 4 h to HL (T 30°C). Control treatment was done with 0.002% Tween 20. After 3 h, the plants were again treated with 200 µM of cPTIO or 0.002% (w/v) Tween 20 (control). Plant leaves were harvested and stored in –80°C.

### Preparation of histones

Histone proteins were extracted with a Histone Purification Kit (Active Motif, Cat No. 40025) either from liquid grown seedlings or from leaf tissue, using manufacturer's instructions with some modifications; 0.5–0.6 g start material was ground to a powder and incubated with 2.5 mL extraction buffer on a rotating platform for 2 h at 4°C. The extracts were centrifuged at maximal RCF at 4°C for 10 min. Afterwards the supernatants were transferred to PD 10 columns (GE Healthcare, Cat No. 17085101), which were previously equilibrated two times with 3.5 mL precooled extraction buffer. The proteins were eluted with 3.5-mL extraction buffer. The eluates were neutralized with one-fourth volumes of 5× neutralization buffer (0.875 mL) to reach a pH of 8. Purification of core histones was performed the same as described in the manufacturer's instruction according to the buffer exchange procedure, using Zeba spin desalting columns 7K MWCO (Thermo Fisher, Cat No. 89882). Columns were prepared by adding 300 µL dH<sub>2</sub>O with a Protease Inhibitor EDTA-free tablet (Roche, Cat No. 04693132001) three times. One hundred microliter of purified core histones were added to the column and centrifuged for 2 min at 1,500g. An amount of histones was measured by NanoDrop 1000 at 230 nm.

### Sodium dodecyl sulfate-polyacrylamide gel electrophoresis

Protein extracts were equally loaded on a precast 12% polyacrylamide (Biorad, Cat No. 4561044) or self-made gel and subjected to a sodium dodecyl sulfate-polyacrylamide gel electrophoresis using a Mini-PROTEAN Electrophoresis cell (Biorad, Cat No. 1658002EDU). Gels were run at 130 V for ~60 min in 1× running buffer. After separation of proteins, a gel was either stained for 30 min with Coomassie brilliant blue solution or further used for a western blot.

### Western blot

Proteins were transferred to a nitrocellulose membrane (Abcam) using a semi-dry western blot system. Prewet membrane and gel were sandwiched between Whatman papers that were presoaked in a transfer buffer. A transfer was performed for 45 min at room temperature (RT). A flow rate of electric charge was dependent on length (L), width (W), and amount (n) of membranes, and was

calculated as follows: mA=L × W × 2.5 × n. An efficient transfer of proteins was determined by staining a membrane with Ponceau S solution (Sigma-Aldrich, Cat No. 6226-79-5). Afterwards a membrane was incubated in a blocking buffer shaking at RT for 1 h, followed by binding with primary antibody in 5% BSA/TBS-T buffer overnight at 4°C. The following antibodies were used for immunodetection of histone marks: acetylated-H3 (1:20,000), acetylated-H3K9 (1:5,000), and acetylated-H3K9/K14 (1:2,000). Anti-FLAG-tag antibody (1:1,000) was used to detect plant-produced FLAG-HDA6. The membrane was washed three times for 5 min with 1× TBS-T buffer, and incubated for 1 h at RT with a horseradish peroxidase-linked secondary antibody in 5% (w/v) BSA/TBS-T buffer. The membrane was washed once with 1× TBS-T and two times with 1× TBS buffer. The signal was developed using Western lightning plus-ECL chemiluminescence substrate (PerkinElmer, Cat No. NEL105001EA).

### Recombinant expression and purification

The vector carrying an N-terminus FLAG-targeted HDA6 (pEarlyGate202/HDA6) was transferred to *E. coli* strain DH5α, followed by electroporation of Agrobacterium strain GV3101 pMP90. Transgenic *Arabidopsis* lines overproducing 3S:FLAG-HDA6 were generated by the floral dip method as described above. Homozygous lines were selected and used for further studies. Plants expressing recombinant FLAG-HDA6 were harvested three weeks after sowing. For analytical studies, around 4 g of ground material were used. Proteins were extracted in two volumes (~8 mL) of CellLyticP buffer (Sigma-Aldrich, Cat No. C2360) supplemented with of the recommended amount of a Protease Inhibitor EDTA-free tablet (Roche, Cat No. 04693132001) by rotating for 1 h at 4°C. Extracts were filtrated trough miracloth (Millipore, Cat No 475855-1R), followed by 15-min centrifugation at 6,000g and 4°C; 60 µL of FLAG-targeted beads (Sigma-Aldrich, Cat No. A2220) were equilibrated with TBS buffer according to the manufacturer's instruction, and added to the extracted proteins. A binding of recombinant protein to the beads was performed by rotating for 4 h at 4°C. Afterwards, the resin was centrifuged for 30 s at 8,200g, and supernatant was discarded. The beads were washed three times with TBS solution and FLAG-HDA6 was eluted with 200 ng/µL of FLAG-Peptide (Sigma-Aldrich, Cat No. F3290) by incubating the resin with synthetic peptide and rotating for 30 min at 4°C.

### Measurement of HDA activity

HDA activity was measured using a commercially available EpigenaseTM HDAC Activity/Inhibition Direct Assay Kit (Epigentek, Cat No. P-4035-48) according to the manufacturer's instruction; 3–17 µL of purified FLAG-HDA6 per well were treated with chemicals such as GSNO, GSH, TSA, DTT, and incubated with 50 ng of substrate for 90 min at RT. HDA-deacetylated product was immunorecognized, and the fluorescence at 530Ex/590Em nm was measured in a fluorescent microplate reader (Tecan infinite 1000). The RFU values were used for relative quantification of HDA activity. HDA

activity was also measured according to (Wegener et al., 2003; 3–17 µL of purified FLAG-HDA6 per well were first treated with GSNO or TSA for 30 min in the dark at RT, followed by incubation with DTT (if it was required) for another 30 min. The HDA reaction was initiated by adding 200 µM of HDA-substrate (Boc-Lys(Ac)-MCA) in 25 µL of HDA buffer, followed by 60-min incubation at 37°C. The reaction was stopped by adding 45 µL of 2× Stopping solution containing 10-mg mL<sup>-1</sup> trypsin and 1-µM TSA. The mixture was incubated for an additional 20 min at 30°C to ensure the tryptic digestion. The release of 7-amino-4-methylcoumarin was measured by monitoring of fluorescence at 380Ex/460Em nm.

### Nitrosothiol and nitrite measurement

S-Nitrosothiols and nitrite were measured using Sievers Nitric Oxide Analyzer NOA 280i (GE Analytical Instruments). The method is based on reduction of SNOs and nitrite to NO, which is further oxidized by ozone to NO<sub>2</sub> (excited state) and O<sub>2</sub>. On the way to the ground state, NO<sub>2</sub> emits chemiluminescence that can be measured by photomultiplier. Approximately 300–500 mg of plant tissue was homogenized in the same volume of PBS solution, and incubated for 20 min at 4°C while rotating. Protein extracts were separated from plant debris by centrifugation for 15 min at maximal speed. For the detection of nitrite 20–100 µL of analyte were injected into triiodide solution. For the detection of SNO content, sulfanilamide (1:9) was added to protein extracts to scavenge nitrite, and 200 µL of the total sulfanilamide-protein extract were injected triiodide solution. Every measurement was performed in duplicate. A standard curve was created with sodium nitrite.

### Measurement of NO emission

NO emission was measured from 3.5 to 4-week-old Arabidopsis plants using a CLD Supreme chemiluminescence analyzer (ECO PHYSICS). The purified measuring gas with a constant flow of 600 mL min<sup>-1</sup> was first conducted through a cuvette containing a plant, and subsequently through the chemiluminescence analyzer. The gas was purified from NO by pulling it through a charcoal column. The CO<sub>2</sub>/H<sub>2</sub>O gas exchange system GFS-3000 (Walz) was equipped with the LED-Array/PAM-Fluorometer 3056-FL for illumination, and connected with an Arabidopsis Chamber 3010-A. Environmental parameters important for plant photosynthesis such as temperature, CO<sub>2</sub> (400 ppm), relative humidity (50%), and light were controlled. Temperature and light were dependent on the experimental setup. For the sunflecks experiment, a plant was first adapted to ambient conditions (200 µmol photons m<sup>-2</sup> s<sup>-1</sup> PPFD and 22°C) for 1 h, and afterwards, a light stress was applied. A sunflecks pattern was created by increasing a light intensity to 1,000 µmol photons m<sup>-2</sup> s<sup>-1</sup> PPFD and temperature to 30°C for 10 min, followed by returning both parameters back to ambient conditions for other 10 min. This pattern was repeated in total four times. In addition, the NO emission of soil

without a plant was measured and subtracted from plant emission.

## Chromatin immunoprecipitation sequencing

### Experimental design

WT and mutant plants were grown under chamber-controlled conditions (10/14-h light/dark) for 4 weeks. By this time, plants achieved similar development stage. At midday (11 am, 5 h after turning on the light) plants were transferred either to dark (D, 0 µmol photons m<sup>-2</sup> s<sup>-1</sup> PPFD, 22°C), LL (200 µmol photons m<sup>-2</sup> s<sup>-1</sup> PPFD, 22°C), or to HL (1,000 µmol photons m<sup>-2</sup> s<sup>-1</sup> PPFD, 30°C) conditions for 4 h. Later, they were harvested and immediately cross-linked.

### Cross-linking

In total, 1–2 g of *Arabidopsis* leaves were put in a 50-mL plastic tube which was then filled with 30 mL precooled crosslinking buffer containing 1% (v/v) formaldehyde. Concentration of suitable formaldehyde amount was obtained experimentally. The tubes were put in a desiccator, and vacuum was applied for 10 min. Crosslinking was stopped by adding glycine to each tube (with the end concentration of 0.125 M) followed by vacuum infiltration for another 5 min. After that, leaves were washed twice with cooled water and dried on paper towels. Collected material was frozen in liquid nitrogen and stored at –80°C.

### Antibody coupling to magnetic beads

For each IP, 20 µL of magnetic beads A were used. Beads of one biological replicate were washed together by pipetting up and down four times with 1 mL buffer RIPA plus protease inhibitor. Afterwards, beads were suspended in the same volume of RIPA. Following that, antibodies were used to immunoprecipitate the following protein–DNA complexes: anti-H3K9/14ac antibody (1 µg/IP), anti-H3K9ac antibody (1 µg/IP), and IgG antibody (1 µg/IP, negative control) were added. Coupling of the antibodies to the beads was performed at 4°C on a rotation platform for ~7 h. In the meantime, chromatin isolation steps were performed. After coupling, the AB-coated beads were washed with 500 µL RIPA for three times and resuspended with the same buffer. The beads were divided into new clean tubes (20 µL/IP).

### Chromatin isolation

Leaves were ground to fine powder with mortar and pestle in liquid nitrogen. A total of 2.3 and 1.3 g of ground materials for ChIP-qPCR and ChIP-seq, respectively, were transferred in a 50 mL plastic tube and mixed with 20-mL Extraction buffer # 1. The suspension was incubated for 15–20 min at 4°C on a rotation platform, followed by centrifugation at 4°C and 2,800g for 20 min. After that, supernatant was removed, and the pellet was suspended with 3 mL NRBT buffer. First 1 mL of buffer was added, and the pellet was suspended with a pipet tip, and then the remaining 2

mL were added. Further, the nuclei were extracted using the same procedure as described above.

### Sonication

After nuclei were isolated, they were carefully suspended (avoiding foam formation) with nuclei sonication buffer. Bioruptor Pico ultrasonic bath and Covaris E220 Evolution were used to shear isolated chromatin for ChIP-qPCR and ChIP-seq, respectively. To perform DNA shearing for ChIP-qPCR, 320  $\mu$ L of sonication buffer were added to nuclei and transferred to 1.5 mL Bioruptor Microtubes (Cat No. C30010016). In total, 14 cycles with 30-s ON/OFF were used. To perform DNA shearing for ChIP-seq, nuclei were resuspended in 220  $\mu$ L of sonication buffer and transferred to micro-Tube AFA Fiber Pre-SlitSnap Cap (Cat No. 520245). The following sonication conditions were used as follows: Peak Incident Power (PIP) – 175, Duty Factor (DF) – 10%, Cycles Per Burst (CPB) – 200, 600 s. After this, sonicated samples were centrifuged for 5 min at 16,000g and 4°C, and the supernatant was used directly for the immunoprecipitation assay or for the detection of shearing efficiency.

### Shearing efficiency

In total, 50 and 20  $\mu$ L of sonicated chromatin for ChIP-qPCR and ChIP-seq, respectively, were diluted to 100  $\mu$ L with sonication buffer. Decrosslinking was performed by adding 6  $\mu$ L of 5-M NaCl, and samples were incubated on a thermoblock for 20 min at 95°C and then centrifuged at RT for 2 min (200g). After that, 2  $\mu$ L of RNaseA were added and samples were incubated for another 40 min at 37°C and then centrifuged at RT for 2 min (200g). DNA was extracted using MinElute PCR purification kit (Qiagen, Cat No. 28004) or by phenol-chloroform followed by ethanol precipitation. DNA was eluted with 11  $\mu$ L of dH<sub>2</sub>O. Concentration was measured using NanoDrop.

### Immunoprecipitation and reverse crosslinking

For ChIP-qPCR, 50  $\mu$ L of sonicated chromatin were diluted with 200  $\mu$ L buffer RIPA (1:5 (v/v)). Ten microliter of diluted chromatin (4% of total) were saved as “Input.” For ChIP-seq, sonicated chromatin was diluted 1:10 (v/v) with RIPA, and 10% was saved as “Input.” The diluted chromatin was added to AB-coated beads and incubated over night at 4°C on a rotating platform. Afterwards, the beads were washed two times with 1 mL of the following buffers: low salt buffer, high salt buffer, LiCl buffer and TE buffer. Each wash step was performed on a rotating platform for 5 min at 4°C. Immunoprecipitated chromatin (IP) was eluted with 125  $\mu$ L of elution buffer plus proteinase inhibitor, incubating on a thermoblock for 15 min at 200g and 65°C. Elution was performed twice, and both eluates were mixed together. For decrosslinking to each “Input,” sample elution buffer was added to reach the same volume as for IP samples (250  $\mu$ L). Decrosslinking was performed by mixing each sample with 10  $\mu$ L of 5 M NaCl (0.2 M NaCl end concentration) and incubating at 65°C for at least 4–5 h at 200 g. After that, samples were treated for 1 h with 4  $\mu$ L of RNaseA (10 mg mL<sup>-1</sup>)

at 37°C. Proteinase K treatment was performed for 2 more hours by adding 2  $\mu$ L Proteinase K (19.2 mg mL<sup>-1</sup>), 5  $\mu$ L of 0.5-M EDTA, and 10  $\mu$ L of 1 M Tris-HCl (pH 6.5). DNA was purified as described above. The DNA was eluted with 21  $\mu$ L of dH<sub>2</sub>O for ChIP-qPCR or 15  $\mu$ L of EB elution buffer (Qiagen, Cat No. 154035622) for ChIP-seq. DNA concentration was measured using Qubit dsDNA HS Assay Kit (Cat No. Q32851).

### Chromatin immunoprecipitation sequencing

Size selection of fragmented DNA was performed using AMPure XP beads (Beckman Coulter, Cat No. A63881) before library preparation. Twenty-one microliters of magnetic beads (1:4:1, ratio of beads to sample) were added to each sample and incubated for 10 min at RT. Afterwards, beads were placed on a magnetic stand and the supernatant was discarded. Beads were washed three times with 20  $\mu$ L of 80% ethanol, and dried. DNA was eluted with 12  $\mu$ L of EB elution buffer by incubating the beads for 3 min. The size of immunoprecipitated and “Input” samples was analyzed using an Agilent High Sensitivity DNA Kit (Cat No. 5067-4626) on an Agilent 2100 Bioanalyzer according to the manufacturing instructions. Library preparation and deep sequencing was performed by IGA Technology Services (<https://igatechnology.com/>) using NextSeq500 and 30 M (75 bp) reads.

### ChIP-seq data analysis

The ChIP-seq reads were aligned against the TAIR10 reference genome assembly for *Arabidopsis* (accessed on May 14, 2018) using bowtie2-2.3.4.1 (Langmead et al., 2009). After quality-based filtering with samtools-1.8 (Li et al., 2009) using -q 2, MACS-1.4.2 (Zhang et al., 2008) was applied for peak calling against the input controls (whole DNA, no ChIP), with genome size 1.35e8, model fold 8,100, fragment size 150 and *P*-value cutoff 1e-5. Differential analysis between groups was performed based on the DESeq2 method (Love et al., 2014) using DiffBind 2.12.0 (Ross-Innes et al., 2012; Stark and Brown, 2019), recentering the peaks at summits and setting the width of consensus peaks to the maximum fragment size estimated by MACS-1.4.2. The alignment format conversion required for DiffBind was done with samtools-1.8 (Li et al., 2009). Differential peaks with adjusted *P*-value (false discovery rate method, FDR) < 0.05 were used for further analyses. Venn diagrams were made with the R package limma, version 3.40.2 (Ritchie et al., 2015), and significance of overlaps was assessed with fisher.test in R version 3.6.0 (Team, 2019). PCA by prcomp and plot functions were employed in R version 3.6.0 (Team, 2019) for visualization of the normalized count data from DiffBind. Read counts for specific genomic locations were queried by samtools-1.8 (Li et al., 2009) and scaled to a common library size of 10e6 for covisualization of ChIP-seq and RNA-seq output.

### Functional enrichment analysis

GO term enrichment for lists of differentially regulated genes was computed in R version 3.6.0 (Team, 2019),

applying fisher.test and p.adjust with the FDR method. The GO terms and annotated genes were taken from org.At.tairGO2ALLTAIRS in the org.At.tair.db R package, version 3.8.2 (Carlson, 2019b). The description of the GO term was obtained from the GO.db R package version 3.8.2 (Carlson, 2019a). Significantly enriched GO terms (FDR < 0.05) were subjected to multidimensional scaling (MDS) analysis by cmdscale in R version 3.6.0 (Team, 2019) using a distance matrix computed with the function dist on binary profiles indicating for each gene of the list whether it is annotated with the respective GO term. Significantly enriched GO terms from the biological process ontology were plotted with respect to the first two MDS coordinates, and colored according to their ancestors among the top level biological process terms, which were classified into five broader categories (response to stimulus: GO:0002376, GO:0023052, GO:0050896; localization: GO:0051179; growth and development: GO:0000003, GO:0008283, GO:0022414, GO:0032501, GO:0032502, GO:0040007, GO:0071840; metabolic process: GO:0008152; other: GO:0001906, GO:0006791, GO:0006794, GO:0007610, GO:0009758, GO:0009987, GO:0015976, GO:0019740, GO:0022610, GO:0040011, GO:0043473, GO:0044848, GO:0048511, GO:0051704, GO:0065007, GO:0098743, GO:0098754, GO:0110148). The visualization was achieved by the R packages ggplot2, version 3.1.1 (Wickham, 2016), and scatterpie, version 0.1.4 (Yu, 2019), as well as the barplot function of R version 3.6.0 (Team, 2019).

## RNA-seq

Wt and mutant plants were grown under chamber-controlled conditions (10/14 h light/dark) for 4 weeks. By this time, plants had achieved a similar development stage. At midday (11 am, 5 h after turning on the light) plants were transferred either to dark (D, 0  $\mu\text{mol}$  photons  $\text{m}^{-2} \text{s}^{-1}$  PPFD, 22°C), LL (200  $\mu\text{mol}$  photons  $\text{m}^{-2} \text{s}^{-1}$  PPFD, 22°C) or to HL (1,000  $\mu\text{mol}$  photons  $\text{m}^{-2} \text{s}^{-1}$  PPFD, 30°C) conditions for 4 h. Later, plants were harvested and stored at -20°C. In total, four biological replicates were analyzed. RNA was extracted using the innuPREP PLANT RNA Kit (Analytik Jena GmbH, Jena Germany) according to the manual. Sequencing libraries were generated from poly(A)-enriched RNA using the NEBNext Ultra II Directional RNA Library Prep kit (New England Biolabs) according to the manufacturer's instructions, and sequenced on an HiSeqV4 instrument (Illumina) as 100-bp single-end reads in a 24-plex pool. Reads were mapped to the TAIR10 reference of Arabidopsis annotated genes ([www.arabidopsis.org](http://www.arabidopsis.org)) using STAR (v2.5.2a; Dobin et al., 2013). Read quantifications were generated using kallisto (v0.43.1; Bray et al., 2016). Differential expression analysis was performed using the DESeq2 package (v1.18.1) with default settings (Love et al., 2014) in R (v3.4.4; Team, 2017).

## Accession numbers

ChIP-seq and RNA-seq data have been deposited in the ArrayExpress functional genomics database at EMBL-EBI

(<https://www.ebi.ac.uk/arrayexpress/experiments/E-MTAB-9299> and <https://www.ebi.ac.uk/arrayexpress/experiments/E-MTAB-9301>, respectively).

## Supplemental data

The following materials are available in the online version of this article.

**Supplemental Figure S1.** Treatment with the NO scavenger cPTIO decreases histone acetylation (H3K9ac).

**Supplemental Figure S2.** Comparison of H3 acetylation after GSNO treatment in wt and *hda6* suspension cells.

**Supplemental Figure S3.** HDAC activity in nuclear extracts of wt and *hda6* cell cultures.

**Supplemental Figure S4.** HDAC activity in *hda6* suspension cells is insensitive to cysteine modifications and TSA.

**Supplemental Table S1.** ChIP-seq and RNA-seq sample and alignment information.

**Supplemental Table S2.** Differentially regulated genes in LL versus D and mutant versus wt comparisons for ChIP-seq and RNA-seq data.

**Supplemental Table S3.** GO term enrichment of LL versus D comparisons for ChIP-seq data.

**Supplemental Table S4.** GO term enrichment of mutant versus wt comparisons for ChIP-seq data.

**Supplemental Table S5.** GO term enrichment of LL versus D comparisons for RNA-seq data.

**Supplemental Table S6.** GO term enrichment of mutant versus wt comparisons for RNA-seq data.

**Supplemental Table S7.** Genes showing enhanced H3K9 acetylation and gene expression for both mutants versus wt under LL conditions.

**Supplemental Table S8.** Genes showing decreased H3K9 acetylation and gene expression for both mutants versus wt under LL conditions.

## Materials availability statement

All unique/stable reagents/plant material generated in this study are available from the Corresponding Author without restriction.

## Data and code availability statements

The ChIP-seq and RNA-seq data generated during this study will be available at ArrayExpress functional genomics database.

## Acknowledgments

We thank Elke Mattes, Lucia Gößl, and Rosina Ludwig for excellent technical assistance.

## Funding

This work was supported by the Bundesministerium für Bildung und Forschung (BMBF).

*Conflict of interest statement.* The authors have no conflicts of interest to declare.

## References

- Ageeva-Kieferle A, Rudolf EE, Lindermayr C** (2019) Redox-dependent chromatin remodeling: a new function of nitric oxide as architect of chromatin structure in plants. *Front Plant Sci* **10**: 625
- An L, Liu Y, Zhang M, Chen T, Wang X** (2005) Effects of nitric oxide on growth of maize seedling leaves in the presence or absence of ultraviolet-B radiation. *J Plant Physiol* **162**: 317–326
- Apelt F, Breuer D, Olas JJ, Annunziata MG, Flis A, Nikoloski Z, Kragler F, Stitt M** (2017) Circadian, carbon, and light control of expansion growth and leaf movement. *Plant Physiol* **174**: 1949–1968
- Avonce N, Leyman B, Mascorro-Gallardo JO, Van Dijck P, Thevelein JM, Iturriaga G** (2004) The Arabidopsis trehalose-6-P synthase AtTPS1 gene is a regulator of glucose, abscisic acid, and stress signaling. *Plant Physiol* **136**: 3649–3659
- Ayyappan V, Sripathi VR, Kalavacharla VK, Saha MC, Thimmapuram J, Bhide KP, Fiedler E** (2019) Genome-wide identification of histone methylation (H3K9me2) and acetylation (H4K12ac) marks in two ecotypes of switchgrass (*Panicum virgatum* L.). *BMC Genomics* **20**: 667
- Bae H, Herman E, Bailey B, Bae H-J, Sicher R** (2005a) Exogenous trehalose alters Arabidopsis transcripts involved in cell wall modification, abiotic stress, nitrogen metabolism, and plant defense. *Physiol Plant* **125**: 114–126
- Bae H, Herman E, Sicher R** (2005b) Exogenous trehalose promotes non-structural carbohydrate accumulation and induces chemical detoxification and stress response proteins in *Arabidopsis thaliana* grown in liquid culture. *Plant Sci* **168**: 1293–1301
- Ballare CL** (2014) Light regulation of plant defense. *Annu Rev Plant Biol* **65**: 335–363
- Bannister AJ, Kouzarides T** (2011) Regulation of chromatin by histone modifications. *Cell Res* **21**: 381–395
- Berr A, Xu L, Gao J, Cognat V, Steinmetz A, Dong A, Shen WH** (2009) SET DOMAIN GROUP25 encodes a histone methyltransferase and is involved in FLOWERING LOCUS C activation and repression of flowering. *Plant Physiol* **151**: 1476–1485
- Besson-Bard A, Gravot A, Richaud P, Auroy P, Duc C, Gaymard F, Taconnat L, Renou JP, Pugin A, Wendehenne D** (2009) Nitric oxide contributes to cadmium toxicity in *Arabidopsis* by promoting cadmium accumulation in roots and by up-regulating genes related to iron uptake. *Plant Physiol* **149**: 1302–1315
- Blanvillain R, Kim JH, Wu S, Lima A, Ow DW** (2009) OXIDATIVE STRESS 3 is a chromatin-associated factor involved in tolerance to heavy metals and oxidative stress. *Plant J* **57**: 654–665
- Bray N, Pimentel H, Melsted H, Pachter L** (2016) Near-optimal probabilistic RNA-seq quantification. *Nature Biotechnology* **34**: 525–527
- Buet A, Simontacchi M** (2015) Nitric oxide and plant iron homeostasis. *Ann N Y Acad Sci* **1340**: 39–46
- Carlson M** (2019a) GO.db: A set of annotation maps describing the entire Gene Ontology. R package version 3.8.2.
- Carlson M** (2019b) org.At.tair.db: Genome wide annotation for *Arabidopsis*. R package version 3.8.2.
- Choe S, Fujioka S, Noguchi T, Takatsuto S, Yoshida S, Feldmann KA** (2001) Overexpression of DWARF4 in the brassinosteroid biosynthetic pathway results in increased vegetative growth and seed yield in *Arabidopsis*. *Plant J* **26**: 573–582
- Choi SM, Song HR, Han SK, Han M, Kim CY, Park J, Lee YH, Jeon JS, Noh YS, Noh B** (2012) HDA19 is required for the repression of salicylic acid biosynthesis and salicylic acid-mediated defense responses in *Arabidopsis*. *Plant J* **71**: 135–146
- Colussi C, Mozzetta C, Gurtner A, Illi B, Rosati J, Straino S, Ragone G, Pescatori M, Zaccagnini G, Antonini A, et al.** (2008) HDAC2 blockade by nitric oxide and histone deacetylase inhibitors reveals a common target in Duchenne muscular dystrophy treatment. *Proc Natl Acad Sci U S A* **105**: 19183–19187
- D'Amico-Damiao V, Carvalho RF** (2018) Cryptochrome-related abiotic stress responses in plants. *Front Plant Sci* **9**: 1897
- Dangl M, Brosch G, Haas H, Loidl P, Lusser A** (2001) Comparative analysis of HD2 type histone deacetylases in higher plants. *Planta* **213**: 280–285
- Delledonne M, Xia Y, Dixon RA, Lamb C** (1998) Nitric oxide functions as a signal in plant disease resistance. *Nature* **394**: 585–588
- Dobin A, Davis CA, Schlesinger F, Drenkow J, Zaleski C, Jha S, Batut P, Chaisson M, Gingeras TR** (2013) STAR: ultrafast universal RNA-seq aligner. *Bioinformatics* **29**: 15–21
- Durner J, Wendehenne D, Klessig DF** (1998) Defense gene induction in tobacco by nitric oxide, cyclic GMP, and cyclic ADP-ribose. *Proc Natl Acad Sci USA* **95**: 10328–10333
- Fancy NN, Bahlmann AK, Loake GJ** (2017) Nitric oxide function in plant abiotic stress. *Plant Cell Environ* **40**: 462–472
- Fares A, Rossignol M, Peltier JB** (2011) Proteomics investigation of endogenous S-nitrosylation in *Arabidopsis*. *Biochem Biophys Res Commun* **416**: 331–336
- Feechan A, Kwon E, Yun BW, Wang Y, Pallas JA, Loake GJ** (2005) A central role for S-nitrosothiols in plant disease resistance. *Proc Natl Acad Sci USA* **102**: 8054–8059
- Feng JH, Jing FB, Fang H, Gu LC, Xu WF** (2011) Expression, purification, and S-nitrosylation of recombinant histone deacetylase 8 in *Escherichia coli*. *Biosci Trends* **5**: 17–22
- Fernandez O, Bethencourt L, Quero A, Sangwan RS, Clement C** (2010) Trehalose and plant stress responses: friend or foe? *Trends Plant Sci* **15**: 409–417
- Floryszak-Wieczorek J, Milczarek G, Arasimowicz M, Ciszewski A** (2006) Do nitric oxide donors mimic endogenous NO-related response in plants? *Planta* **224**: 1363–1372
- Govind SR, Jogaiah S, Abdelrahman M, Shetty HS, Tran LS** (2016) Exogenous trehalose treatment enhances the activities of defense-related enzymes and triggers resistance against Downy Mildew disease of pearl millet. *Front Plant Sci* **7**: 1593
- Graf A, Schlereth A, Stitt M, Smith AM** (2010) Circadian control of carbohydrate availability for growth in *Arabidopsis* plants at night. *Proc Natl Acad Sci USA* **107**: 9458–9463
- Griebel T, Zeier J** (2008) Light regulation and daytime dependency of inducible plant defenses in *Arabidopsis*: phytochrome signaling controls systemic acquired resistance rather than local defense. *Plant Physiol* **147**: 790–801
- Grundy J, Stoker C, Carre IA** (2015) Circadian regulation of abiotic stress tolerance in plants. *Front Plant Sci* **6**: 648
- Gupta KJ, Igamberdiev AU, Kaiser WM** (2010) New insights into the mitochondrial nitric oxide production pathways. *Plant Signal Behav* **5**: 999–1001
- He GM, Zhu XP, Elling AA, Chen LB, Wang XF, Guo L, Liang MZ, He H, Zhang HY, Chen FF, et al.** (2010) Global epigenetic and transcriptional trends among two rice subspecies and their reciprocal hybrids. *Plant Cell* **22**: 17–33
- He Y, Tang RH, Hao Y, Stevens RD, Cook CW, Ahn SM, Jing L, Yang Z, Chen L, Guo F, et al.** (2004) Nitric oxide represses the *Arabidopsis* floral transition. *Science* **305**: 1968–1971
- Helliwell CA, Wood CC, Robertson M, James Peacock W, Dennis ES** (2006) The *Arabidopsis* FLC protein interacts directly in vivo with SOC1 and FT chromatin and is part of a high-molecular-weight protein complex. *Plant J* **46**: 183–192
- Hess DT, Matsumoto A, Kim SO, Marshall HE, Stampler JS** (2005) Protein S-nitrosylation: purview and parameters. *Nat Rev Mol Cell Biol* **6**: 150–166
- Hollender C, Liu Z** (2008) Histone deacetylase genes in *Arabidopsis* development. *J Integr Plant Biol* **50**: 875–885
- Holzmeister C, Frohlich A, Sarioglu H, Bauer N, Durner J, Lindermayr C** (2011) Proteomic analysis of defense response of wildtype *Arabidopsis thaliana* and plants with impaired NO-hemeostasis. *Proteomics* **11**: 1664–1683
- Hu J, Huang X, Chen L, Sun X, Lu C, Zhang L, Wang Y, Zuo J** (2015) Site-specific nitrosoproteomic identification of endogenously S-nitrosylated proteins in *Arabidopsis*. *Plant Physiol* **167**: 1731–1746

- Huang X, von Rad U, Durner J** (2002) Nitric oxide induces transcriptional activation of the nitric oxide-tolerant alternative oxidase in *Arabidopsis* suspension cells. *Planta* **215**: 914–923
- Illi B, Dello Russo C, Colussi C, Rosati J, Pallaoro M, Spallotta F, Rotili D, Valente S, Ragone G, Martelli F, et al.** (2008) Nitric oxide modulates chromatin folding in human endothelial cells via protein phosphatase 2A activation and class II histone deacetylases nuclear shuttling. *Circ Res* **102**: 51–58
- Jaenisch R, Bird A** (2003) Epigenetic regulation of gene expression: how the genome integrates intrinsic and environmental signals. *Nat Genet* **33**: 245–254
- Jain P, von Toerne C, Lindermayr C, Bhatia SC** (2018) S-nitrosylation/denitrosylation as a regulatory mechanism of salt stress sensing in sunflower seedlings. *Physiol Plant* **162**: 49–72
- Jasid S, Simontacchi M, Bartoli CG, Puntarulo S** (2006) Chloroplasts as a nitric oxide cellular source. Effect of reactive nitrogen species on chloroplastic lipids and proteins. *Plant Physiol* **142**: 1246–1255
- Jeong RD, Kachroo A, Kachroo P** (2010) Blue light photoreceptors are required for the stability and function of a resistance protein mediating viral defense in *Arabidopsis*. *Plant Signal Behav* **5**: 1504–1509
- Karmodiya K, Krebs AR, Oulad-Abdelghani M, Kimura H, Tora L** (2012) H3K9 and H3K14 acetylation co-occur at many gene regulatory elements, while H3K14ac marks a subset of inactive inducible promoters in mouse embryonic stem cells. *BMC Genomics* **13**: 424
- Kim B, Fujioka S, Kwon M, Jeon J, Choe S** (2013) *Arabidopsis* brassinosteroid-overproducing gulliver3-D/dwarf4-D mutants exhibit altered responses to jasmonic acid and pathogen. *Plant Cell Rep* **32**: 1139–1149
- Ko ML, Shi L, Huang CC, Grushin K, Park SY, Ko GY** (2013) Circadian phase-dependent effect of nitric oxide on L-type voltage-gated calcium channels in avian cone photoreceptors. *J Neurochem* **127**: 314–328
- Kovacs I, Holzmeister C, Wirtz M, Geerlof A, Frohlich T, Romling G, Kuruthukulangarakoola GT, Linster E, Hell R, Arnold GJ, et al.** (2016) ROS-mediated inhibition of S-nitrosoglutathione reductase contributes to the activation of anti-oxidative mechanisms. *Front Plant Sci* **7**: 1669
- Kovacs I, Lindermayr C** (2013) Nitric oxide-based protein modification: formation and site-specificity of protein S-nitrosylation. *Front Plant Sci* **4**: 137
- Kozlov AV, Staniek K, Nohl H** (1999) Nitrite reductase activity is a novel function of mammalian mitochondria. *FEBS Lett* **454**: 127–130
- Kuruthukulangarakoola GT, Zhang J, Albert A, Winkler B, Lang H, Buegger F, Gaupels F, Heller W, Michalke B, Sarioglu H, et al.** (2017) Nitric oxide-fixation by non-symbiotic haemoglobin proteins in *Arabidopsis thaliana* under N-limited conditions. *Plant Cell Environ* **40**: 36–50
- Kwon E, Feechan A, Yun BW, Hwang BH, Pallas JA, Kang JG, Loake GJ** (2012) AtGSNOR1 function is required for multiple developmental programs in *Arabidopsis*. *Planta* **236**: 887–900
- Langmead B, Trapnell C, Pop M, Salzberg SL** (2009) Ultrafast and memory-efficient alignment of short DNA sequences to the human genome. *Genome Biol* **10**: R25
- Latrasse D, Jegu T, Li H, de Zelicourt A, Raynaud C, Legras S, Gust A, Samajova O, Veluchamy A, Rayapuram N, et al.** (2017) MAPK-triggered chromatin reprogramming by histone deacetylase in plant innate immunity. *Genome Biol* **18**: 131
- Lee U, Wie C, Fernandez BO, Feelisch M, Vierling E** (2008) Modulation of nitrosative stress by S-nitrosoglutathione reductase is critical for thermotolerance and plant growth in *Arabidopsis*. *Plant Cell* **20**: 786–802
- Li H, Handsaker B, Wysoker A, Fennell T, Ruan J, Homer N, Marth G, Abecasis G, Durbin R, Genome Project Data Processing Subgroup** (2009) The sequence alignment/map format and SAMtools. *Bioinformatics* **25**: 2078–2079
- Li J, Nam KH, Vafeados D, Chory J** (2001) BIN2, a new brassinosteroid-insensitive locus in *Arabidopsis*. *Plant Physiol* **127**: 14–22
- Lindermayr C, Rudolf EE, Durner J, Groth M** (2020) Interactions between metabolism and chromatin in plant models. *Mol Metab* **38**: 100951
- Liu L, Hausladen A, Zeng M, Que L, Heitman J, Stamler JS** (2001) A metabolic enzyme for S-nitrosothiol conserved from bacteria to humans. *Nature* **410**: 490–494
- Liu P, Zhang H, Yu B, Xiong L, Xia Y** (2015) Proteomic identification of early salicylate- and flg22-responsive redox-sensitive proteins in *Arabidopsis*. *Sci Rep* **5**: 8625
- Love MI, Huber W, Anders S** (2014) Moderated estimation of fold change and dispersion for RNA-seq data with DESeq2. *Genome Biol* **15**: 550
- Luo M, Tai R, Yu CW, Yang S, Chen CY, Lin WD, Schmidt W, Wu K** (2015) Regulation of flowering time by the histone deacetylase HDA5 in *Arabidopsis*. *Plant J* **82**: 925–936
- Machado-Nils AV, de Faria LO, Vieira AS, Teixeira SA, Muscara MN, Ferrari EA** (2013) Daily cycling of nitric oxide synthase (NOS) in the hippocampus of pigeons (*C. livia*). *J Circadian Rhythms* **11**: 12
- Mahrez W, Arellano MS, Moreno-Romero J, Nakamura M, Shu H, Nanni P, Köhler C, Gruissem W, Hennig L** (2016) H3K36ac is an evolutionary conserved plant histone modification that marks active genes. *Plant Physiol* **170**: 1566–1577
- Mata CG, Lamattina L** (2001) Nitric oxide induces stomatal closure and enhances the adaptive plant responses against drought stress. *Plant Physiol* **126**: 1196–1204
- Matiolli CC, Tomaz JP, Duarte GT, Prado FM, Del Bem LE, Silveira AB, Gauer L, Correa LG, Drumond RD, Viana AJ, et al.** (2011) The *Arabidopsis* bZIP gene AtbZIP63 is a sensitive integrator of transient abscisic acid and glucose signals. *Plant Physiol* **157**: 692–705
- Mazza CA, Ballare CL** (2015) Photoreceptors UVR8 and phytochrome B cooperate to optimize plant growth and defense in patchy canopies. *New Phytol* **207**: 4–9
- Mengel A, Ageeva A, Georgii E, Bernhardt J, Wu K, Durner J, Lindermayr C** (2017) Nitric oxide modulates histone acetylation at stress genes by inhibition of histone deacetylases. *Plant Physiol* **173**: 1434–1452
- Minard ME, Jain AK, Barton MC** (2009) Analysis of epigenetic alterations to chromatin during development. *Genesis* **47**: 559–572
- Mur LA, Mandon J, Persijn S, Cristescu SM, Moshkov IE, Novikova GV, Hall MA, Harren FJ, Hebelstrup KH, Gupta KJ** (2013) Nitric oxide in plants: an assessment of the current state of knowledge. *AoB Plants* **5**: pls052
- Murfett J, Wang XJ, Hagen G, Guilfoyle TJ** (2001) Identification of *Arabidopsis* histone deacetylase HDA6 mutants that affect transgene expression. *Plant Cell* **13**: 1047–1061
- Nott A, Watson PM, Robinson JD, Crepaldi L, Riccio A** (2008) S-Nitrosylation of histone deacetylase 2 induces chromatin remodelling in neurons. *Nature* **455**: 411–415
- Okuda K, Ito A, Uehara T** (2015) Regulation of histone deacetylase 6 activity via S-nitrosylation. *Biol Pharm Bull* **38**: 1434–1437
- Pandey R, Muller A, Napoli CA, Selinger DA, Pikaard CS, Richards EJ, Bender J, Mount DW, Jorgensen RA** (2002) Analysis of histone acetyltransferase and histone deacetylase families of *Arabidopsis thaliana* suggests functional diversification of chromatin modification among multicellular eukaryotes. *Nucleic Acids Res* **30**: 5036–5055
- Parani M, Rudrabhatla S, Myers R, Weirich H, Smith B, Leaman DW, Goldman SL** (2004) Microarray analysis of nitric oxide responsive transcripts in *Arabidopsis*. *Plant Biotechnol J* **2**: 359–366
- Planchet E, Jagadis Gupta K, Sonoda M, Kaiser WM** (2005) Nitric oxide emission from tobacco leaves and cell suspensions: rate limiting factors and evidence for the involvement of mitochondrial electron transport. *Plant J* **41**: 732–743
- Polverari A, Molesini B, Pezzotti M, Buonauro R, Marte M, Delle Donne M** (2003) Nitric oxide-mediated transcriptional

- changes in *Arabidopsis thaliana*. *Mol Plant Microbe Interact* **16**: 1094–1105
- Puyaubert J, Baudouin E** (2014) New clues for a cold case: nitric oxide response to low temperature. *Plant Cell Environ* **37**: 2623–2630
- Puyaubert J, Fares A, Reze N, Peltier JB, Baudouin E** (2014) Identification of endogenously S-nitrosylated proteins in *Arabidopsis* plantlets: effect of cold stress on cysteine nitrosylation level. *Plant Sci* **215–216**: 150–156
- Riens B, Heldt HW** (1992) Decrease of nitrate reductase activity in spinach leaves during a light-dark transition. *Plant Physiol* **98**: 573–577
- Ritchie ME, Phipson B, Wu D, Hu Y, Law CW, Shi W, Smyth GK** (2015) Limma powers differential expression analyses for RNA-sequencing and microarray studies. *Nucleic Acids Res* **43**: e47
- Rockel P, Strube F, Rockel A, Wildt J, Kaiser WM** (2002). Regulation of nitric oxide (NO) production by plant nitrate reductase in vivo and in vitro. *J Exp Bot* **53**: 103–110
- Romero-Puertas MC, Campostrini N, Matte A, Righetti PG, Perazzoli M, Zolla L, Roepstorff P, Delledonne M** (2008) Proteomic analysis of S-nitrosylated proteins in *Arabidopsis thaliana* undergoing hypersensitive response. *Proteomics* **8**: 1459–1469
- Ross-Innes CS, Stark R, Teschendorff AE, Holmes KA, Ali HR, Dunning MJ, Brown GD, Gojis O, Ellis IO, Green AR, et al.** (2012) Differential oestrogen receptor binding is associated with clinical outcome in breast cancer. *Nature* **481**: 389–393
- Sakamoto A, Ueda M, Morikawa H** (2002) *Arabidopsis glutathione-dependent formaldehyde dehydrogenase* is an S-nitrosoglutathione reductase. *FEBS Lett* **515**: 20–24
- Sano S, Aoyama M, Nakai K, Shimotani K, Yamasaki K, Sato MH, Tojo D, Suwastika IN, Nomura H, Shiina T** (2014) Light-dependent expression of flg22-induced defense genes in *Arabidopsis*. *Front Plant Sci* **5**: 531
- Schwartzman JM, Thompson CB, Finley LWS** (2018) Metabolic regulation of chromatin modifications and gene expression. *J Cell Biol* **217**: 2247–2259
- Stark R, Brown G** (2019) DiffBind: differential binding analysis of ChIP-Seq peak data. <http://bioconductor.org/packages/release/bioc/vignettes/DiffBind/inst/doc/DiffBind.pdf>
- Stoimenova M, Igamberdiev AU, Gupta KJ, Hill RD** (2007) Nitrite-driven anaerobic ATP synthesis in barley and rice root mitochondria. *Planta* **226**: 465–474
- RC Team** (2017) R: A Language and Environment for Statistical Computing. <https://www.R-project.org/>
- RC Team** (2019) R: A Language and Environment for Statistical Computing. R Foundation for Statistical Computing
- Tessadori F, van Zanten M, Pavlova P, Clifton R, Pontvianne F, Snoek LB, Millenaar FF, Schulkes RK, van Driel R, Voesenek LA, et al.** (2009) Phytochrome B and histone deacetylase 6 control light-induced chromatin compaction in *Arabidopsis thaliana*. *PLoS Genet* **5**: e1000638
- Tian QY, Sun DH, Zhao MG, Zhang WH** (2007) Inhibition of nitric oxide synthase (NOS) underlies aluminum-induced inhibition of root elongation in *Hibiscus moscheutos*. *New Phytol* **174**: 322–331
- Trapet P, Kulik A, Lamotte O, Jeandroz S, Bourque S, Nicolas-Frances V, Rosnoble C, Besson-Bard A, Wendehenne D** (2015) NO signaling in plant immunity: a tale of messengers. *Phytochemistry* **112**: 72–79
- van der Woude LC, Perrella G, Snoek BL, van Hoogdalem M, Novak O, van Verk MC, van Kooten HN, Zorn LE, Tonckens R, Dongus JA, et al.** (2019) HISTONE DEACETYLASE 9 stimulates auxin-dependent thermomorphogenesis in *Arabidopsis thaliana* by mediating H2A.Z depletion. *Proc Natl Acad Sci USA* **116**: 25343–25354
- Vanzo E, Merl-Pham J, Velikova V, Ghirardo A, Lindermayr C, Hauck SM, Bernhardt J, Riedel K, Durner J, Schnitzler JP** (2016) Modulation of protein S-nitrosylation by isoprene emission in poplar. *Plant Physiol* **170**: 1945–1961
- Wegener D, Wirsching F, Riester D, Schwienhorst A** (2003) A fluorogenic histone deacetylase assay well suited for high-throughput activity screening. *Chem Biol* **10**: 61–68
- Wickham H** (2016) ggplot2: Elegant Graphics for Data Analysis. Springer, New York
- Widiez T, Symeonidi A, Luo CY, Lam E, Lawton M, Rensing SA** (2014) The chromatin landscape of the moss *Physcomitrella patens* and its dynamics during development and drought stress. *Plant J* **79**: 67–81
- Wu K, Zhang L, Zhou C, Yu CW, Chaikam V** (2008) HDA6 is required for jasmonate response, senescence and flowering in *Arabidopsis*. *J Exp Bot* **59**: 225–234
- Wünsche H, Baldwin IT, Wu J** (2011) S-Nitrosoglutathione reductase (GSNOR) mediates the biosynthesis of jasmonic acid and ethylene induced by feeding of the insect herbivore *Manduca sexta* and is important for jasmonate-elicited responses in *Nicotiana attenuata*. *J Exp Bot* **62**: 4605–4616
- Xu F, Copeland C** (2012) Nuclear extraction from *Arabidopsis thaliana*. *Bio Protocols* **2**:306
- Xu S, Guerra D, Lee U, Vierling E** (2013). S-nitrosoglutathione reductases are low-copy number, cysteine-rich proteins in plants that control multiple developmental and defense responses in *Arabidopsis*. *Front Plant Sci* **4**: 430
- Xue Y, Liu Z, Gao X, Jin C, Wen L, Yao X, Ren J** (2010) GPS-SNO: computational prediction of protein S-nitrosylation sites with a modified GPS algorithm. *PLoS One* **5**: e11290
- Yu CP, Lin JJ, Li WH** (2016) Positional distribution of transcription factor binding sites in *Arabidopsis thaliana*. *Sci Rep* **6**: 25164
- Yu CW, Liu X, Luo M, Chen C, Lin X, Tian G, Lu Q, Cui Y, Wu K** (2011) HISTONE DEACETYLASE6 interacts with FLOWERING LOCUS D and regulates flowering in *Arabidopsis*. *Plant Physiol* **156**: 173–184
- Yu G** (2019) scatterpie: Scatter Pie Plot. R Package Version 0.1.4. <https://CRAN.R-project.org/package=scatterpie>
- Yu M, Lamattina L, Spoel SH, Loake GJ** (2014) Nitric oxide function in plant biology: a redox cue in deconvolution. *New Phytol* **202**: 1142–1156
- Zhang H, Lang Z, Zhu JK** (2018) Dynamics and function of DNA methylation in plants. *Nat Rev Mol Cell Biol* **19**: 489–506
- Zhang Y, Liu T, Meyer CA, Eeckhoute J, Johnson DS, Bernstein BE, Nusbaum C, Myers RM, Brown M, Li W, et al.** (2008) Model-based analysis of ChIP-Seq (MACS). *Genome Biol* **9**: R137
- Zhao LQ, Zhang F, Guo JK, Yang YL, Li BB, Zhang LX** (2004) Nitric oxide functions as a signal in salt resistance in the calluses from two ecotypes of reed. *Plant Physiol* **134**: 849–857
- Zhao M, Zhao X, Wu Y, Zhang L** (2007) Enhanced sensitivity to oxidative stress in an *Arabidopsis* nitric oxide synthase mutant. *J Plant Physiol* **164**: 737–745